PERGAMON

Planetary and Space Science 47 (1999) 1243–1262

Planetary and Space Science

A comparison of the atmospheres of Jupiter and Saturn: deep atmospheric composition, cloud structure, vertical mixing, and origin

S.K. Atreya[a,*], M.H. Wong[a], T.C. Owen[b], P.R. Mahaffy[c], H.B. Niemann[c], I. de Pater[d], P. Drossart[e], Th Encrenaz[e]

[a]*Department of Atmospheric, Oceanic and Space Sciences, The University of Michigan, Ann Arbor, MI 48109-2143, USA*
[b]*Institute for Astronomy, University of Hawaii, Honolulu, HI 96822, USA*
[c]*Goddard Space Flight Center, Greenbelt, MD 20771, USA*
[d]*Department of Astronomy, University of California at Berkeley, Berkeley, CA 94720, USA*
[e]*DESPA, Observatoire de Paris, F-92195, Meudon, France*

Received 9 December 1998; received in revised form 22 February 1999; accepted 22 March 1999

Abstract

We present our current understanding of the composition, vertical mixing, cloud structure and the origin of the atmospheres of Jupiter and Saturn. Available observations point to a much more vigorous vertical mixing in Saturn's middle-upper atmosphere than in Jupiter's. The nearly cloud- free nature of the Galileo probe entry site, a 5-micron hotspot, is consistent with the depletion of condensible volatiles to great depths, which is attributed to local meteorology. Somewhat similar depletion of water may be present in the 5-micron bright regions of Saturn also. The supersolar abundances of heavy elements, particularly C and S in Jupiter's atmosphere and C in Saturn's, as well as the progressive increase of C from Jupiter to Saturn and beyond, tend to support the icy planetesimal model of the formation of the giant planets and their atmospheres. However, much work remains to be done, especially in the area of laboratory studies, including identification of possible new microwave absorbers, and modelling, in order to resolve the controversy surrounding the large discrepancy between Jupiter's global ammonia abundance, hence the nitrogen elemental ratio, derived from the earth-based microwave observations and that inferred from the analysis of the Galileo probe-orbiter radio attenuation data for the hotspot. We look forward to the observations from Cassini–Huygens spacecraft which are expected to result not only in a rich harvest of information for Saturn, but a better understanding of the formation of the giant planets and their atmospheres when these data are combined with those that exist for Jupiter.

1. Introduction

Important constraints can be placed on the models of the formation of Jupiter and Saturn and the subsequent origin of their atmospheres by a comparative study of their deep atmospheric composition, vertical mixing, and the cloud structure. In this paper, those species that can determine the abundances of heavy elements, especially O, C, N and S, are investigated in detail as they are central to the question of the formation of the giant planets and their atmospheres. Their distribution with depth can also provide important clues to local meteorology and dynamics. Because of observational limitations, the structure of clouds is poorly known on both planets. Therefore, condensation models are necessary for characterizing the cloud structure, at least to the first order, and for interpreting the available observations. Information on the atmospheric vertical transport is derived largely from the analysis of the height profiles of various hydrocarbons near the homopause, and ammonia and phosphine near the tropopause. In the following sec-

* Corresponding author.
E-mail address: atreya@umich.edu (S.K. Atreya)

0032-0633/99/$20.00
PII: S0032-0633(99)00047-1

tions, we will discuss the interrelated questions of composition, mixing, clouds, and origin, by comparing and analyzing the current information for the atmospheres of Jupiter and Saturn.

2. Composition

Remote sensing, fly-by observations with the Voyager infrared and ultraviolet spectrometers between 1979 and 1989 have provided some of the most comprehensive data on the composition of the atmospheres of the giant planets. Observations made by the Infrared Space Observatory (ISO) from earth-orbit in 1995–1998 have confirmed some of these measurements, and furthered our knowledge of the composition by the detection of several new species in the stratospheres, including water vapor on all four giant planets, CO_2 on Jupiter, Saturn and Neptune, benzene (C_6H_6) on Jupiter and Saturn, and diacetylene (C_4H_2) on Saturn. A comprehensive discussion of the ISO measurements and techniques is presented elsewhere in this issue (Encrenaz et al., 1999). Ground-based observations at infrared, submm, mm, and radio wavelengths have resulted in complementary data and useful information on ammonia, H_3^+, and several disequilibrium species. The first direct in situ measurement of the composition of Jupiter's deep atmosphere was carried out by the Galileo Probe Mass Spectrometer (GPMS) from 0.5 to 21 bar. A detailed discussion of the GPMS measurement techniques and data reduction has been published elsewhere (Niemann et al., 1998). A complete listing of the current best values of species mixing ratios in the atmospheres of Jupiter and Saturn is given in Table 1. In this paper we will focus on those species that are relevant to the questions of cloud formation, local meteorology, mixing, and the origin of the atmospheres of Jupiter and Saturn.

The condensible volatiles in the atmospheres of both Saturn and Jupiter are ammonia (NH_3), hydrogen sulfide (H_2S), and water vapor (H_2O). Ammonia condenses into NH_3 ice, H_2S reacts with NH_3 to form ammonium hydrosulfide, NH_4SH, or ammonium sulfide, $(NH_4)_2S$, and water condenses to water ice or an aqueous ammonia solution. Water is expected to form the deepest and most substantial clouds, and the clouds of NH_4SH and NH_3-ice will form above the water cloud (discussed in Section 4). The Galileo probe detected a tenuous cloud at 0.5 bar, another at 1.34 bar, a thin cloud of minor vertical extent at 1.6 bar, and an even more tenuous particulate structure near 2.5–3.6 bar (Ragent et al., 1998; Sromovsky et al., 1998). As discussed in Section 4, this unexpected behavior is consistent with the depletion of the condensible volatiles seen by the GPMS and other instruments on the Galileo probe. It is remarkable that the condensible volatiles were all depleted in the upper troposphere; however, their mixing ratios continued to build with depth. In the case of NH_3 and H_2S, the mixing ratios leveled off to constant values deep in the atmosphere, whereas the H_2O mixing ratio was most likely still increasing even at the 20 bar level (the deepest part probed) where it was measured by the GPMS as subsolar, so that the well-mixed deep atmospheric abundance of water is still an unknown.

Even prior to Galileo, numerous attempts were made to determine the abundance of water in Jupiter's deep atmosphere through remote sensing in the 5-μm spectral region. However, the interpretation of these data was controversial, with values ranging from highly subsolar (Drossart and Encrenaz, 1982; Bjoraker et al., 1986; Lellouch et al., 1989; West et al., 1986) to 2 × solar (Carlson et al., 1993). Drossart and Encrenaz (1982) modeled five H_2O lines for comparison with the average of all Voyager 1 IRIS 5-μm spectra for latitudes of $\pm 30^\circ$, and found that their analysis is consistent with a water vapor distribution with a mixing ratio $(q_{H_2O}) = 10^{-5}$ (or 0.006 × solar) with all the water restricted to levels where $T \geq 250$ K. Bjoraker et al. (1986) used a higher spectral resolution dataset from the Kuiper Airborne Observatory (KAO) to distinguish between strong, medium, and weak water lines in the 5-μm spectrum, which allowed them to constrain the vertical variation of q_{H_2O}. Their favored profile, based on KAO observations spanning the $\pm 40^\circ$ latitudes of Jupiter, featured subsaturated q_{H_2O} at $p \geq 2$ bar, increasing to 3.3×10^{-5} (0.02 × solar) at 6 bar. Bjoraker et al. (1986) also analyzed Voyager IRIS data to look for spatial variation in the q_{H_2O} profile. The variation they retrieved applied only to pressures < 4 bars, where they found the NEB (North Equatorial Belt) to be more depleted in water than other regions. They found no difference in the deepest retrieved abundances of water between spectral ensembles at different latitudes, all of which were fit by the same deep abundance derived from their KAO analysis. New laboratory measurements of the NH_3 spectrum near 5 μm justified a new analysis of the IRIS spectra by Lellouch et al. (1989), who also obtained a constant q_{H_2O} of several times 10^{-6} at levels deeper than 230 K, depending on spectral ensemble. Carlson et al. (1993) simultaneously fit IRIS 45 and 5-μm spectra using a complex radiative transfer model with many new features, including multiple-scattering, thermally-emitting clouds with spectrally-dependent extinction, and cloud base levels determined by their assumed condensible volatile abundances. They argued that the slope of the IRIS spectra required the presence of a water cloud. Although they admitted that their analysis did not allow the unique determination of the deep well-mixed water abundance, the link in their model between the required water cloud base

Table 1
Composition of the atmospheres of Jupiter and Saturn[a]

Species	Mixing ratios relative to H_2	
	Jupiter	Saturn
Major species		
H_2	1.0	1.0
He	0.157 ± 0.0036 (a,b)	0.034 ± 0.028 (c)
Principal minor species		
H_2O	Global: see text (d,e), $\leq 10^{-6}$ ($\leq$4 bar, hotspot) (b), $5.6 \pm 2.5 \times 10^{-5}$ (12 bar, hotspot) (b), $6 \pm 3 \times 10^{-4}$ (19 bar, hotspot) (b), $2–20 \times 10^{-9}$ (upper stratosphere) (g)	Greatly subsaturated ($p \geq 3$ bars) (f), $2–20 \times 10^{-9}$ ($p < 0.3$ mb) (g)
CH_4	$2.1 \pm 0.4 \times 10^{-3}$ (b)	$4.5(+2.4, -1.9) \times 10^{-3}$ (h)
CH_3		$1.5–7.5 \times 10^{13}$ cm^{-2} (stratosphere) (i)
C_2H_6	$1–5 \times 10^{-6}$ (stratosphere) (j,k)	$3 \pm 1 \times 10^{-6}$ (stratosphere) (h,l)
C_2H_2	$3–10 \times 10^{-8}$ (stratosphere) (m,n), $<2.5 \times 10^{-6}$ (1–10 μbar) (j)	$2.1 \pm 1.4 \times 10^{-7}$ (stratosphere/20–50 mb, northern hemisphere) (h), $5 \pm 1 \times 10^{-8}$ (southern hemisphere) (h)
C_2H_4	$7 \pm 3 \times 10^{-9}$ (north polar region) (o)	
C_3H_4	$2.5(+2, -1) \times 10^{-9}$ (north polar region) (o)	6×10^{-10} ($<$10 mb) (l)
C_3H_8	Detection (b)	
C_4H_2		9×10^{-11} (10 mb) (l)
C_6H_6	$2(+2, -1) \times 10^{-9}$ (stratosphere, north polar region) (o), Detection (global average) (p)	2.5×10^{-10} cm^{-2} (global average/stratosphere) (p)
NH_3	Global: see text (q), $\sim 0.2–1 \times 10^{-5}$ (0.5–2 bar, hotspot) (r), $3.3 \pm 1.5 \times 10^{-4}$ (4 bar, hotspot) (s), $8.1 \pm 1.16 \times 10^{-4}$ ($\geq$8 bar, hotspot) (s)	$\sim 6 \times 10^{-4}$ (global) (q)
H_2S	$< 1 \times 10^{-7}$ ($\leq$4 bar) (b), 7×10^{-6} (8.7 bar) (b), $7.7 \pm 0.5 \times 10^{-5}$ ($\geq$16 bar) (b)	$< 2 \times 10^{-7}$ (t,u)
Disequilibrium species		
PH_3	$1–2 \times 10^{-7}$ (0.2–0.6 bar), 6×10^{-7} ($>$1 bar) (w,x)	$7(+3, -2) \times 10^{-6}$ ($>$400 mb) (v), $3 \pm 1 \times 10^{-6}$ (100–1000 mb) (y)
CO	1.6×10^{-9} (z)	$1 \pm 0.3 \times 10^{-9}$ (v)
CO_2	Detection ($<$10 mb) (l)	3×10^{-10} ($<$10 mb) (l)
GeH_4	$7 \pm 2 \times 10^{-10}$ (w)	$4 \pm 4 \times 10^{-10}$ (v)
AsH_3	$2.2 \pm 1.1 \times 10^{-10}$ (aa)	$3 \pm 1 \times 10^{-9}$ (v)
Other minor constituents		
H	Variable (ab,ac)	
$(H_2)_2$	Variable (ad,ae)	
H_3^+	Variable (af)	
HCl		1.1×10^{-9} (tentative) (ag)
Cl	Tentative detection (b)	

[a] Mixing ratios are given relative to H_2, in order to facilitate comparison to the solar values. Mole fractions may be calculated by dividing the species number density by the atmospheric number density, thus the mole fractions of H_2 and He in Jupiter's atmosphere, e.g., are, 0.864 and 0.136, respectively. In the case of Saturn, mixing ratios and mole fractions are nearly equal because of the very low helium abundance. Isotopic and noble gas results are listed in Table 2. (a) von Zahn et al. (1998), (b) Niemann et al. (1998), (c) Conrath et al. (1984), (d) Supersolar values were reported by Carlson et al. (1993), however, this result is controversial, (e) Subsolar values are reported by others (Drossart and Encrenaz, 1982; Bjoraker et al. 1986; Lellouch et al. (1989); Roos-Serote et al., 1999) who reanalyzed the same Voyager IRIS data as Carlson et al. (1993) as well as other data (see text), (f) Drossart (1998), (g) Feuchtgruber et al. (1997), (h) Courtin et al. (1984), (i) Bézard et al. (1998), (j) Festou et al. (1981), (k) Kostiuk et al. (1983), (l) de Graauw et al. (1997), (m) Noll et al. (1986), (n) Hanel et al. (1979), (o) Kim et al. (1985), (p) Bézard (1998), value given as column abundance since the exact pressure level in the stratosphere is uncertain, (q) de Pater and Massie (1985), Fouchet et al. (1999), (r) Sromovsky et al. (1998), (s) Folkner et al. (1998), (t) Owen et al. (1977), (u) Caldwell (1977), (v) Noll and Larson (1991), (w) Kunde et al. (1982), (x) Encrenaz et al. (1978), (y) Weisstein and Serabyn (1994), (z) Noll et al. (1988), (aa) Noll and Larson (1990), (ab) Judge and Carlson (1974), (ac) Broadfoot et al. (1979), (ad) Gautier et al. (1983), (ae) Frommhold and Birnbaum (1984), (af) Drossart et al. (1989), Kim et al. (1991), Baron et al. (1991), (ag) Weisstein and Serabyn (1996).

level and q_{H_2O} led them to derive a preferred abundance of 2 × solar for water in the deep mixed atmosphere. The Carlson et al. (1993) analysis was the only one to require a water cloud in NEB hot spots. A comparison between the Voyager infrared (IRIS), Galileo orbiter near-infrared (NIMS), and ISO/SWS 5-μm spectra of Jupiter (Roos-Serote et al., 1999) (SWS, Short Wavelength Spectrometer) revealed an anoma-

lous slope in the continuum level shortward of 5 μm in the IRIS spectra, of the right sense to give the impression of a water cloud in the Carlson et al. (1993) model. Apart from a possible calibration problem in the IRIS spectra, Roos-Serote et al. (1999) also implied from their analysis that the problem of the retrieval of H_2O abundance in the deep mixed atmosphere from 5-μm spectra is too intricately coupled to the assumptions about the structure and opacity of clouds to permit a unique solution. In other words, inferences about the water mixing ratio in the deep atmosphere from remote sensing at 5 μm are highly questionable. The Galileo NIMS spectra themselves are consistent with subsaturated and subsolar q_{H_2O} profiles between 4 and 8 bar (Roos-Serote et al., 1998), in agreement with the GPMS measurements (Niemann et al., 1998). The NIMS data also show that water vapor is highly variable from place to place on Jupiter. It is due to this non-uniform distribution, along with the abovementioned difficulties of interpreting the 5-μm spectra, that to this day it is not possible to determine the global abundance of water on Jupiter from remote sensing observations. Although it was hoped that the Galileo probe would penetrate to levels where the deep atmospheric mixing ratio of water could be sampled, there is still no definitive result available for the deep atmospheric mixing ratio of water in Jupiter's atmosphere.

The ISO observations of Saturn at 5 μm indicate that, as in Jupiter's 5-μm hotspot where the Galileo probe made its measurements, water vapor is greatly subsaturated at $p \geq 3$ bars (Drossart, 1998). Unlike the Galileo probe's localized measurements, the ISO observations are globally or hemispherically averaged. Nevertheless, it would be premature to conclude that water is subsaturated everywhere on Saturn since the thermal emission from Saturn's warm/hot regions is expected to dominate the globally averaged 5-μm spectra, as is found to be the case with Jupiter where the thermal emission from the hot spots dominates the disk-averaged 5-μm spectra despite the relatively small area of the planet the hot spots cover (Orton et al., 1996; Owen and Westphal, 1972; Gillett et al., 1969). The Cassini orbiter observations may not be sufficient to settle beyond doubt the question of the water mixing ratio in the deep atmosphere, i.e. below the water clouds of Saturn.

Earth-based observations failed to detect H_2S in the atmospheres of Jupiter and Saturn. The greatly subsolar upper limits in the 1-bar region seem to imply loss of this species through condensation at deeper levels (Section 4). Indeed, condensation seems inevitable, given the large mixing ratio of H_2S measured by the GPMS in the deep atmosphere of Jupiter (Fig. 1). At the 16-bar level in the Galileo probe entry site, the H_2S mixing ratio is 7.7×10^{-5}, or $2.5 \times$ solar. This should then be the global H_2S mixing ratio below the ammonium hydrosulfide cloud base (Section 4) outside the 5-μm hot spot where the Galileo probe entered. Since the Cassini orbiter instruments can only measure H_2S above the NH_4SH clouds, any inference of its

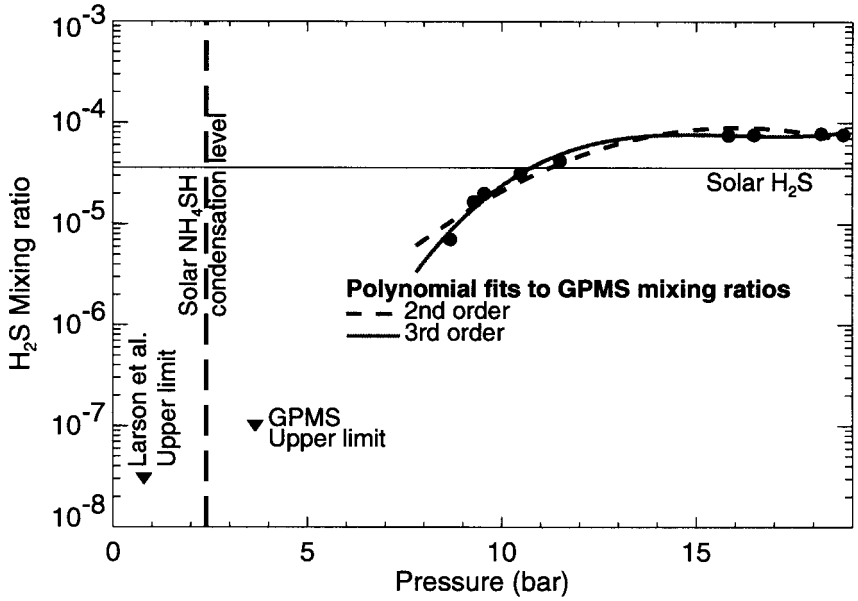

Fig. 1. GPMS measurements of the H_2S mixing ratio are shown by squares at pressures greater than 8 bars. No compositional measurements were done by GPMS between 3.8 and 8 bars. The H_2S count rates are statistically insignificant at pressures below 3.8 bars, so that only an upper limit for H_2S could be obtained at 3.8 bars (triangle). The upper limit shown at 0.8 bar (triangle) is from the ground-based infrared studies of Larson et al. (1984). Also shown are second and third order polynomial fits to the GPMS data beyond 8 bars. H_2S mixing ratio corresponding to solar S/H (Table 2), and the expected atmospheric level of NH_4SH condensation (Fig. 4) for this sulfur abundance, are indicated.

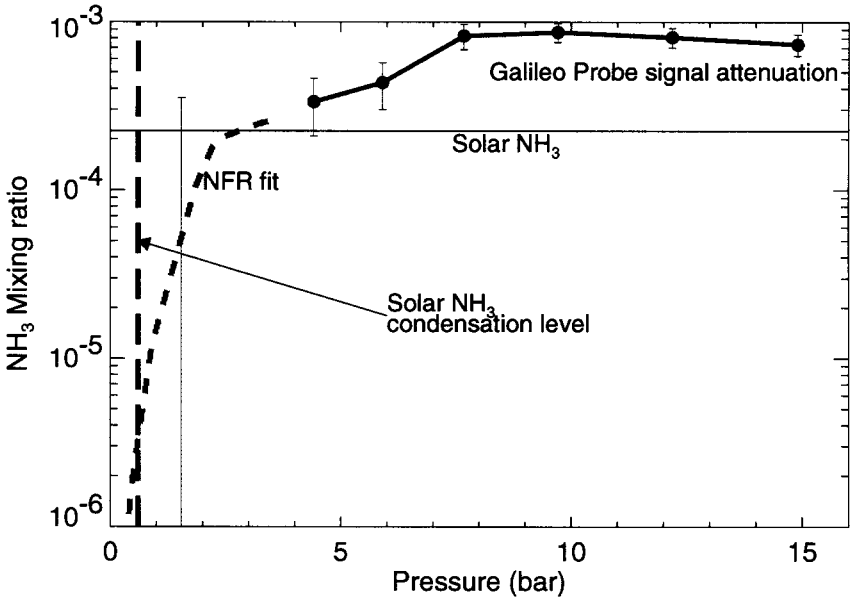

Fig. 2. The NH_3 profiles from Net Flux Radiometer measurements (Sromovsky et al. 1998) and from probe signal attenuation measurements (Folkner et al. 1998) are shown. NH_3 mixing ratio corresponding to solar N/H (Table 2), and the expected atmospheric level of NH_3 condensation (Fig. 4) for this ammonia abundance, are indicated.

mixing ratio in Saturn's deep atmosphere will be model dependent.

On the other hand, there is a good likelihood that the NH_3 mixing ratio will be measured to considerable depths in Saturn's atmosphere with infrared instruments on board the Cassini orbiter. Presently, the best estimates on its abundance below the clouds are from the Very Large Array (VLA) measurements. These ground-based global observations in the microwave give supersolar NH_3 in Saturn's atmosphere, although the uncertainty is large (de Pater and Massie, 1985). Similar radio observations of Jupiter at several wavelengths ranging from 0.5 mm to 20 cm yield a 'disk-averaged' ammonia mixing ratio of 1–1.3 × solar at pressures greater than approximately 1–2 bars in the Jovian atmosphere (de Pater and Massie, 1985; ratio to solar based on the current solar $N/H = 1.12 \times 10^{-4}$). These data also reveal nonuniformities in the distribution of ammonia over the planet, with ammonia being subsolar and subsaturated down to 1.8–2 bar level in the belts and subsolar and subsaturated down to about 1 bar level in the zones (de Pater, 1986); the ammonia clouds are located at 750 ± 200 mb (Banfield et al., 1998). The only available 'in situ' results on the NH_3 abundance in Jupiter's atmosphere have been derived from an analysis of Galileo probe's Net Flux Radiometer data in the 0.5–3 bar region (Sromovsky et al., 1998), and to about 15 bars from an analysis of the attenuation of the probe to orbiter radio signal at 21.6 cm (Folkner et al., 1998), as shown in Fig. 2. The Galileo probe radio observations yield depleted levels of NH_3 in the upper parts; but at the depth where the NH_3 mixing ratio appears to level off in these data ($p \approx 8$–10 bars), its value was measured to be $(3.6 \pm 0.5) \times$ solar (Folkner et al., 1998).[1] Finally, a preliminary analysis of the recent ISO/SWS 'global' observations of Jupiter at 5 μm (Fouchet et al., 1999) appear to be consistent down to 4 bars (the ISO data do not extend below 4 bars) with the NH_3 profile derived by Folkner et al. (1998) for the Galileo probe entry site—a 5-μm hotspot. (Comparison was made with the 'central' values of NH_3 in the Galileo probe data, but the error bars in the radio data in this pressure range are substantial). Although global, the ISO observations should be regarded as being heavily weighted by emission from the hotspots since they were done at 5 μm. Nevertheless, it is remarkable that all of the above observations, the disk-averaged ground-based radio data, the Galileo probe radio data for the hotspot, and the ISO/SWS 5-μm data, yield subsaturated and subsolar levels of ammonia to some depth and, within the range of experimental uncertainties, similar values of the NH_3 mixing ratio at the 4 bar level, ranging from 1–1.3 × solar for the disk-averaged ground-based radio data to 1.3 × solar for the Galileo probe radio data to 1.6 × solar for ISO/SWS data. Despite this agreement in the upper regions of the troposphere, it is clear that the localized Galileo

[1] Note that Folkner et al. (1998) report a value of $(4 \pm 0.5) \times$ solar, instead, which results from their use of a solar $N/H = 1 \times 10^{-4}$. Using their NH_3 'mole fraction' of 700 ± 100 ppm, and the solar $N/H = 1.12 \times 10^{-4}$ (Anders and Grevesse, 1989), we find that the Folkner et al. (1998) NH_3 changes to $(3.6 \pm 0.5) \times$ solar.

probe results on ammonia (Folkner et al., 1998) as a whole are in disagreement with the globally averaged ground-based radio data (de Pater and Massie, 1985).

In order to understand whether the highly supersolar NH_3 measured for the deep atmosphere of Jupiter by Folkner et al. (1998) in the Galileo probe region could also be valid elsewhere on Jupiter, we have carried out a calculation to simulate the microwave spectrum from 0.5 mm to 20 cm for comparison with the disk-averaged ground-based radio results of de Pater and Massie (1985). At these wavelengths, the main source of opacity is ammonia gas, which has a broad absorption band near 1.23 cm. We model this opacity using Spilker's (1990, 1993) formulism. Spilker's (1998) new formulism is very similar to the lineshape used by de Pater and Mitchell (1993) and in this paper, and will not noticeably affect the model spectra presented here (Spilker, personal communication, 1999). At wavelengths longward of 6 cm, absorption by water vapor and water droplets becomes increasingly important, while at mm wavelengths collision-induced absorption by hydrogen gas and extinction by ammonia cloud particles becomes noticeable (see e.g., de Pater and Mitchell, 1993). Since H_2O follows the saturated vapor curve over most of the altitudes probed at radio wavelengths, the brightness temperature varies only slightly (few K at 20 cm) when the H_2O abundance is increased from solar up to 20 times solar, if the absorptivity by cloud particles is ignored. If the latter effect is included, depending on the cloud density the brightness temperature can be influenced noticeably. The absorption lines of H_2S are broadened considerably under high pressure (de Boer and Steffes, 1994), but absorptivity on Jupiter at the pressure levels probed is negligible. Nevertheless, absorption by both water and hydrogen sulfide is included in our model.

Fig. 3a shows the ground-based radio data and the simulated microwave spectra based on the thermochemical equilibrium cloud condensation model (described in Section 4), assuming, below the clouds,

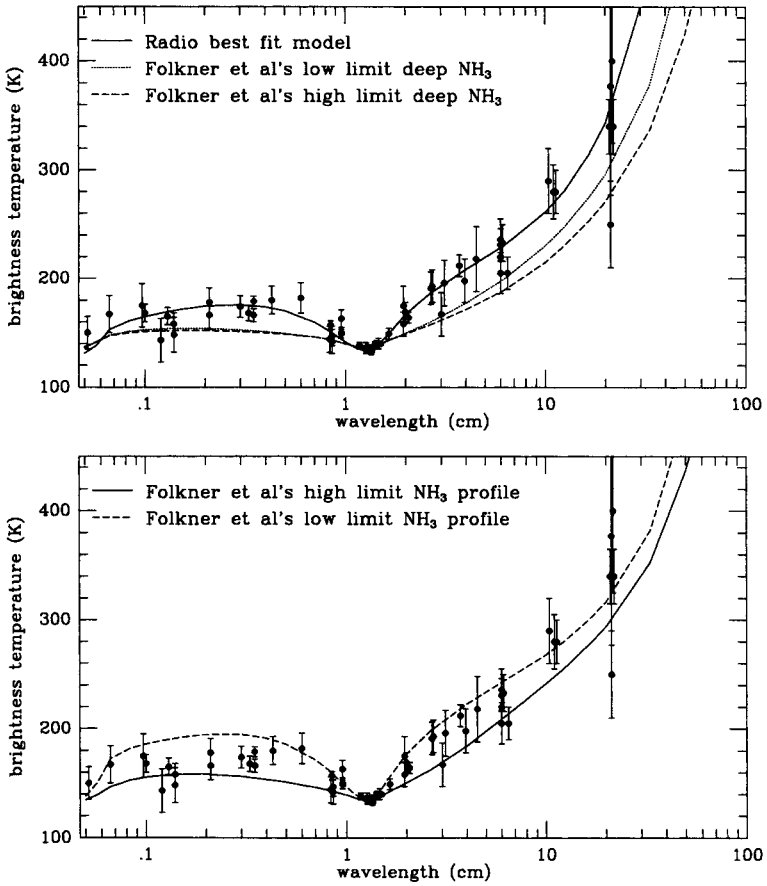

Fig. 3. (a, top) Minimum and maximum values for deep NH_3 were taken from Folkner et al. (1998) and used as inputs for the ECCM. The resulting ammonia profile was used in the radiative transfer code to produce the simulated microwave spectra. Data points are taken from de Pater and Massie (1985). The best fit model corresponds to 1.2 × solar ammonia below the ammonia-ice clouds. (b, bottom) Comparison of microwave spectra calculated using Folkner et al.'s (1998) NH_3 'profiles' and the ground-based radio data of de Pater and Massie (1985). Fig. 3 is adapted from de Pater et al. (1999).

C: 3 × solar, S: 2 × solar, O: 2 × solar, and N: varying from Folkner et al.'s (1998) minimum value of 2.8 × solar to their maximum value of 4.4 × solar in the deep atmosphere.[2] It is clear that both at the cm and the mm wavelengths, the two curves based on Folkner et al.'s N/H are inconsistent with the ground-based microwave data. In fact, the calculated curves may depart from the microwave data of Fig. 3a even more, particularly at the mm wavelength, if absorption by cloud particles is included in the model. The best fit to the ground-based microwave data is obtained with 1.2 × solar NH_3 as shown in Fig. 3a. [Such a simulation was first presented by Romani et al., 1995, and was based on the cloud model of Atreya and Romani (1985) and a radiative transfer model as described in de Pater et al. (1989). The calculated spectra shown in this paper (Fig. 3) are based on current cloud models and abovementioned Spilker's (1990, 1993) formulism, whose details will be presented elsewhere (de Pater et al., 1999). Absorption by cloud particles is included in these models.] Finally, if we assume that *everywhere* on Jupiter, NH_3 has the 'profile' reported by Folkner et al. (1998) for the Galileo probe region, i.e. depleted above and recovering in the deep atmosphere, then we produce microwave spectra shown in Fig. 3b for Folkner et al.'s low and high limits on ammonia at each depth. As seen in this figure, the two curves straddle the ground-based microwave data, therefore any model that fits these data points would be consistent with Folkner et al.'s NH_3 profiles also.

In view of the results of the above exercise of simulating the microwave spectra, it is evident that we are faced with two extreme scenarios, (a) that NH_3 is in approximately solar mixing ratio from below its condensation level (~0.7 bar) to the deep atmosphere, as is required by the ground-based radio data (de Pater and Massie, 1985), but which is clearly contradictory to the Galileo probe results (Folkner et al., 1998), or (b) that *everywhere* on Jupiter, the NH_3 mixing ratio with depth follows a *profile* like the one measured by Folkner et al. in the Galileo probe region. Folkner et al.'s profile requires a large loss of NH_3 gas at pressures < 8 bars. In principle, NH_3 gas may be removed by dissolving it in a (liquid) water cloud or by forming an ammonium hydrosulfide (NH_4SH) ice cloud (Section 4). However, in the Galileo probe region, no water clouds were detected, and the purported NH_4SH cloud was too tenuous to take out any appreciable amount of NH_3. In the regions outside the hotspot (where the Galileo probe entered) also, it is inconceivable that the abovementioned clouds could be a significant sink of the ammonia gas, since it requires an unacceptably high supersolar abundance of water, and similar concentrations of NH_3 and H_2S contrary to the results of Galileo probe measurements. Finally, although Folkner et al.'s (1998) ammonia profile with depth may be related to local meteorology (Section 4), we know of no convincing dynamical processes that could result in such a profile everywhere on Jupiter, so we must discard (b) as a serious possibility. A further argument against the applicability of Folkner et al.'s profile everywhere on Jupiter comes from the observations of ammonia clouds from Earth and space. Over most of Jupiter, relatively thick clouds of ammonia are observed at a pressure of ~750 mb (e.g. Banfield et al., 1998), consistent with the predictions of equilibrium cloud condensation model for 1.2 × solar NH_3 (Section 4). Folkner et al.'s (1998) ammonia profile, on the other hand, would permit only very thin wispy clouds of ammonia or essentially a cloud-free atmosphere, as was indeed the case in the hot spot to which these data pertain, but inconsistent with the global observations of ammonia clouds on Jupiter.

Since neither of the two scenarios (a) or (b) can satisfactorily reconcile the ground-based and the Galileo probe data on ammonia, we will look into other possibilities, including the role of other sources of microwave opacity, and inhomogeneities in the ammonia distribution. The presence of an unaccounted-for microwave absorber *may* be able to reconcile possibility (a) with the conclusions of Folkner et al. (1998). This idea is appealing, especially in view of the recent laboratory measurements suggesting that current models seriously underestimate the cm wavelength opacity of PH_3 (Hoffman et al., 1999; Steffes, personal communication, 1998). In order to reduce Folkner et al.'s (1998) 3.6 × solar NH_3 to solar (the global value measured from the ground), approximately 10 × solar PH_3 would have to be present in Jupiter's deep atmosphere ($p > 5$ bars), according to these authors. However, the current values of the PH_3 mixing ratios at 1 bar are essentially solar (Table 1). We find it difficult to see how P could be enhanced by ~3 × more than C or S, even in the deep atmosphere. In any event, continuing analysis of the GPMS data is expected to firm up the PH_3 mixing ratio in the deep atmosphere. Finally, despite the reservations we have about the required high PH_3 abundance in the deep atmosphere, the possibility of microwave absorption by PH_3 (or other absorbers) should be regarded as viable at this time. This is because the present laboratory data on the PH_3 microwave absorption (Hoffman et al., 1999) already show considerable wavelength and pressure dependence. However, these measurements were done at room temperature and at pressures of only up to 5 bars, both of which are much lower than

[2] We have chosen a somewhat wider range for NH_3, $(3.6 \pm 0.8) \times$ solar, than Folkner et al.'s (1998) $(3.6 \pm 0.5) \times$ solar (footnote 1), in order to account for the scatter in their data (fig. 11 of Folkner et al. (1998); data plotted also in Fig. 2 of this paper).

those corresponding to the level of Folkner et al.'s (1998) deep atmospheric ammonia data. In summary, only after the full microwave absorption spectrum of PH_3 becomes available from ongoing laboratory studies, will it be possible to calculate detailed model spectra and thus evaluate the role of PH_3 (or another absorber) in determining the ammonia mixing ratio profile in Jupiter's deep atmosphere. Until that happens, some other microwave absorber is identified, or some as yet unknown factors (such as a better understanding of the non-thermal (synchrotron) emission from Jupiter's radiation belts at wavelengths $\geq$6 cm, possible loss of ammonia in supercooled water, etc.) affect the model spectra, it seems reasonable, for the time being, to regard the ground-based radio observation results of the deep atmospheric ammonia mixing ratio of 1–1.3 $\times$ solar as being representative of the globally averaged NH_3 in Jupiter's atmosphere, with a caveat that values as large as 3.6 $\times$ solar obtained in the deep atmosphere from an analysis of Galileo probe's radio data are a strong possibility. This last possibility arises from the fact that the disk-averaged microwave spectra, hence the interpretation of ammonia abundance in the deep atmosphere from the global data, may be influenced by inhomogeneities in the NH_3 distribution, belt-zone differences and the depletion of ammonia down to the 1 bar level in the zones and down to about 2 bar level in the belts as reported by de Pater (1986), as well as perhaps by other factors as mentioned above. Further work will be required to resolve this important question.

The heavy element abundances can provide useful constraints for models explaining the formation of the giant planets. In addition to O, N, and S, as discussed above, carbon and phosphorus elemental ratios have been measured on both Jupiter and Saturn. The Galileo probe measurement of CH_4 (Niemann et al., 1998) confirms earlier results (Gautier and Owen, 1989) that the carbon elemental ratio is enhanced by a factor of 3 relative to solar in Jupiter's atmosphere. The Voyager IRIS measurements show that it may be enhanced by a factor of 6 relative to solar in Saturn's atmosphere, although the uncertainty associated with this measurement is large (Courtin et al., 1984). However, a precise measurement of CH_4 on Saturn is expected with the Cassini infrared spectrometer, CIRS. This is largely due to the limb sounding capability of CIRS, in addition to its higher sensitivity in the middle infrared compared to the Voyager infrared instrument, IRIS. By limb sounding, the contribution functions for the H_2 S(1) line can be pushed upward in the stratosphere to just overlap those for the ν_4 band of CH_4 viewed in the nadir mode. This gives the redundancy to separate the effects of temperature and CH_4 abundance, which the Voyager IRIS did not have (M. Flasar, personal communication, 1999). It is expected that with CIRS the CH_4 abundance in Saturn's atmosphere can be determined with the same accuracy as with IRIS at Jupiter, which agrees well with the Galileo Probe mass spectrometer data. Ground-based observations indicate that unlike Jupiter, the mixing ratio of PH_3 is much greater than solar in Saturn's atmosphere (Table 1; Noll and Larson, 1991; Weisstein and Serabyn, 1994). The uncertainties in these data are, however, large, and there are substantial discrepancies between different measurements covering similar atmospheric pressure regions. We will have to wait for the infrared observations from Cassini to settle this important measurement. The Galileo probe mass spectrometer measured the abundances of Ne, Ar, Kr and Xe for the first time in Jupiter's atmosphere. No data on these noble gases are available in Saturn's atmosphere, nor are they expected from Cassini observations. On the other hand, helium, which is presently poorly constrained in Saturn's atmosphere, is expected to be measured more accurately by the Cassini infrared and radio instruments. A highly subsolar abundance of Ne was measured in Jupiter's atmosphere by the GPMS. It is believed to result from the removal of this gas by liquid helium into which it dissolves, and is carried with the helium raindrops as they fall into the planetary interior (Roulston and Stevenson, 1995). Similar depletion of neon in Saturn's atmosphere is expected, but as mentioned above Ne will not be measured by the Cassini instruments. The current best estimates on xenon and krypton mixing ratios in Jupiter's atmosphere are, respectively, $(2.5 \pm 0.7) \times$ solar and $(3 \pm 1) \times$ solar (Mahaffy et al., 1998b), following the recent laboratory enrichment cell studies with the experimental unit (the refurbished flight spare Galileo probe mass spectrometer). Further refinements in the noble gas abundances are expected as results of ongoing laboratory calibration work become available. Our current understanding of the elemental and isotopic abundances in the atmospheres of Jupiter and Saturn is summarized in Table 2.

Table 1 lists many trace constituents, including disequilibrium species (PH_3, GeH_4, AsH_3 and CO) and hydrocarbons in addition to methane. Arsine (AsH_3) is found to be much more abundant in Saturn's atmosphere than in Jupiter's (Noll and Larson, 1991), as is the case with phosphine. Whereas the presence of above disequilibrium species in the upper tropospheres and stratospheres of Jupiter and Saturn is most likely the result of strong upward convection from the deep interiors of these planets where they are in thermochemical equilibrium, the distributions of the hydrocarbons and ammonia in the atmosphere are governed to a large extent by loss processes following the photochemical changes they undergo mainly in the stratosphere. The loss processes of the photochemically produced trace species include, in particular, vertical

Table 2
Elemental and isotopic abundances[a]

Elements	Sun (a)	Jupiter/Sun	Saturn/Sun
Elemental ratios			
^{4}He/H	0.0975	0.807 ± 0.02	$\sim 0.2 \pm 0.1$
^{20}Ne/H	1.15×10^{-4}	0.10 ± 0.01 (b)	
^{36}Ar/H	3.05×10^{-6}	1.7 ± 0.6 (b)	
^{84}Kr/H	9.20×10^{-10}	3.0 ± 1.0 (c)	
^{132}Xe/H	4.45×10^{-11}	2.5 ± 0.7 (c)	
C/H	3.62×10^{-4}	2.9 ± 0.5	~ 6
N/H	1.12×10^{-4}	Global: see text Hotspot: 3.6 ± 0.5	2–4(?)
O/H	8.51×10^{-4}	Global: see text 0.033 ± 0.015 (hotspot, 12 bars) 0.35 (hotspot, 19 bars)	
P/H	3.73×10^{-7}	0.82	4–9
S/H	1.62×10^{-5}	2.5 ± 0.15	
Isotopic ratios			
Elements	Sun	Jupiter	Saturn
^{13}C/^{12}C	0.011	0.0108 ± 0.0005 (b)	0.011 (d)
^{3}He/^{4}He	$1.5 \pm 0.3 \times 10^{-4}$ (e,f,g,h) (meteoritic)	$1.66 \pm 0.05 \times 10^{-4}$ (i)	
D/H	$3.0 \pm 0.17 \times 10^{-5}$ (j), $2.6 \pm 1.0 \times 10^{-5}$ (h)	$2.6 \pm 0.7 \times 10^{-5}$ (i), $1.8(+1.1, -0.5) \times 10^{-5}$ (k,l)	$2.3 \pm 1 \times 10^{-5}$ (l,m)

[a] References not found in Table 1: (a) Anders and Grevesse (1989), (b) Niemann et al. (1996, 1998), (c) Mahaffy et al. (1998b), (d) Combes et al. (1977), (e) Black (1972), (f) Eberhardt (1974), (g) Geiss and Reeves (1972), (h) Geiss (1993), (i) Mahaffy et al. (1998a), (j) Gautier and Morel (1997), (k) Lellouch et al. (1997), (l) Encrenaz et al. (1999), (m) Griffin et al. (1996).

transport followed by condensation (for some species) in the stratospheres and in the vicinity of the tropopause cold trap of Jupiter and Saturn. Certain trace gases, such as H_2O, H_2S and NH_3, on the other hand, are removed through condensation even deeper in the troposphere. In the next sections we discuss our current understanding of these processes in the atmospheres of Jupiter and Saturn.

3. Vertical mixing

Vertical mixing plays a central role in determining the distribution of species in planetary atmospheres from their region of production to the deep atmosphere. It is parameterized by the eddy diffusion coefficient, K, and the distribution of species is related to vertical mixing through the following continuity equation:

$$\frac{\mathrm{d}\phi_i}{\mathrm{d}z} = P_i - L_i$$

where ϕ_i is the flux of the i-th constituent, and P_i and L_i are its production and loss rates, and ϕ_i is given by:

$$\phi_i = n_i\left[-K\left(\frac{1}{n_i}\frac{\mathrm{d}n_i}{\mathrm{d}z} + \frac{1}{H_a} + \frac{1}{T}\frac{\mathrm{d}T}{\mathrm{d}z}\right) - D_i\left(\frac{1}{n_i}\frac{\mathrm{d}n_i}{\mathrm{d}z} + \frac{1}{H_i} + \frac{1}{T}\frac{\mathrm{d}T}{\mathrm{d}z}\right)\right]$$

n_i and H_i are constituent number density and scale height, respectively, and H_a and T are atmospheric (mean) scale height and temperature. K and D are eddy and molecular diffusion coefficients. The expressions for the scale heights are,

$$H_i = RT/M_i g,\ H_a = RT/M_a g$$

M_i and M_a are, respectively, the molecular weights of the constituent and the atmosphere (i.e. mean), g is gravity, and R is the Gas Constant.

Whereas the molecular diffusion coefficient, D, may be determined both from laboratory measurements of gas diffusion, and theoretically from gas kinetic considerations, no such reliable means exists for determining the eddy mixing coefficient. For K, one must rely largely on measurements of the height distributions of trace gases. Sometimes certain spectral emissions can be exploited to derive information on K. For the atmospheres of Jupiter and Saturn, resonance emissions of He 584 Å and H Ly-α (121.6 nm) were used on Voyager, but with limited success mainly due to the very low intensity of the former, and to the fact that methane (CH_4) absorbs Ly-α in the case of the latter. In the atmospheres of all four giant planets, K has been determined at least near the homopause level by the technique of ultraviolet solar and stellar occultation on Voyager (see Atreya (1986) for a comprehen-

Table 3
Eddy diffusion coefficient, K[a]

Planet	K (cm^2 s^{-1})	Density (cm^{-3})	Pressure (bar)	Altitude (km)
Jupiter	$1.4(+0.8, -0.7) \times 10^6$ (a)	1.4×10^{13}	10^{-6}	385 (homopause)
	4.6×10^2 (b)	9.3×10^{18}	0.14	40 (troposphere)
	1.5×10^4 (b)	2.4×10^{19}	0.42	20 (troposphere)
Saturn	$1.7(+4.3, -1.0) \times 10^8$ (c)	1.2×10^{11}	5×10^{-9}	1140 (homopause)
	$8.0(+4.0, -4.0) \times 10^7$ (d)			(homopause)
	$\geq 10^8$ (e)			(homopause)
	$\leq 3.5 \times 10^3$ (f)	1.1×10^{19}	0.13	80 (troposphere, 40° N)
	$\leq 8.7 \times 10^3$ (f)	1.1×10^{19}	0.13	80 (troposphere, 12° N)
Uranus	$5–10 \times 10^3$ (g,h,i)	$2–1 \times 10^{15}$	$4–2 \times 10^{-5}$	354–390 (homopause)
Neptune	$3–10 \times 10^6$ (j)	$\sim 10^{13}$	2×10^{-7}	585–610 (homopause)

[a] (a) Atreya et al. (1981): Voyager UV solar/stellar occultation data on hydrocarbons, (b) The tropospheric K's are derived from the HST/FOS UV data on ammonia (Edgington et al., 1999, which includes an update on the values published previously by Edgington et al. (1998). The values listed are typical for equatorial and midlatitude regions, and have an uncertainty of a factor of 3. Interhemispherical and latitudinal differences up to a factor of 5 in the values of K have been found, (c) Atreya (1982): Voyager UV solar/stellar occultation data on hydrocarbons, and H Ly-α (121.6 nm) emission, (d) Sandel et al. (1982): Voyager UV solar/stellar occultation data on hydrocarbons, and He 584 Å emission, (e) Parkinson et al. (1998): Voyager He 584 Å emission data, (f) Edgington et al. (1997): Upper limits on K from the HST/FOS UV data on phosphine, (g) Encrenaz et al. (1998): ISO/global data on acetylene, (h) Atreya et al. (1991): Voyager UV solar occultation data on hydrocarbons, (i) Bishop et al. (1990): Voyager UV solar occultation data on hydrocarbons, (j) Bishop et al. (1998): Voyager UV solar occultation data on hydrocarbons.

sive discussion of the measurement techniques; see Table 3 for a listing of successful measurements of K for all four giant planets, alongwith the measurement techniques and the references). These measurements refer mostly to the equatorial and low latitudes. The vertical distribution of a minor trace constituent, usually acetylene (C_2H_2) and sometimes CH_4, is measured by the occultation technique. The measured distribution is then compared with model distributions obtained by solving the above continuity equation with K varied as a free parameter. Sometimes, the calculated distributions of the trace constituents are used to simulate the observed occultation light curves, again holding K as a free parameter in the model. This technique then allows one to fix both the value of the eddy diffusion coefficient as well as its variation with altitude. This method of determining K requires a good knowledge of the photochemical process responsible for the production and loss of the species in the atmosphere. Fortunately, for the most part the method has been quite successful in establishing the values of the eddy mixing coefficient in the atmospheres of all four giant planets. A controversy about K derived from the He 584 Å emission in Saturn's atmosphere has also been resolved recently. A reanalysis of the Saturn He 584 Å data using radiative transfer models with partial frequency redistribution and an inhomogeneous atmospheric model has led Parkinson et al. (1998) to conclude that the earlier analysis of the same data by Smith et al. (1983) was incorrect so that, within the range of uncertainty, the eddy diffusion coefficient Parkinson et al. (1998) obtain is in agreement with the results of other techniques, most notably the occultation technique (Atreya, 1982), not a factor of 100 smaller value reported by Smith et al. (1983). The only other new data relevant to K in the upper atmosphere of Saturn come from global observations of CH_4 and CH_3 by the Short Wavelength Spectrometer on the ISO satellite. A preliminary analysis of the CH_4 fluorescence in the ν_3 band between 3.2 and 3.4 μm measured by ISO/SWS gives disk-averaged values of K at the homopause of Saturn that are compatible with those measured by the Voyager occultation technique (Drossart et al., 1999). Similarly, it has been argued that the column abundance of the methyl radical (CH_3), which was detected for the first time in Saturn's atmosphere by ISO/SWS (Bézard et al., 1998), is compatible with the accepted Voyager values of K (Atreya et al., 1999; Ollivier et al., 1999). An order of magnitude discrepancy between the measured CH_3 column abundance and that given by photochemical models (Bézard et al., 1998) is most likely due to the use of too low a rate for the CH_3 loss reactions in the models (Atreya et al., 1999; Ollivier et al., 1999).

Only recently has it been possible to determine with some degree of confidence the strength of vertical mixing in the lower atmospheres of Jupiter and Saturn. From measurements of the tropospheric height profiles of ammonia (NH_3) on Jupiter and phosphine (PH_3) on Saturn with the Hubble Space Telescope/ Faint Object Spectrograph in the 180–230 nm range, compared to the photochemical model results, Edgington et al. (1997, 1998, 1999) derive the values of K in the tropospheres of these two planets. Our present understanding of the eddy mixing coefficients in the atmospheres of Jupiter and Saturn, along with a comparison with the values for the other two giant planets, is summarized in Table 3. Although the Jupiter and Saturn

values differ by almost a factor of 100 at the homopause, the variation of K with the atmospheric number density, n, is found to be quite similar, i.e., $K \propto n^{-a}$, where $0.5 \leq a \leq 0.6$. It is not obvious why the strength of vertical mixing in Saturn's upper atmosphere is $100\times$ more than in Jupiter's. Previously, it has been surmised that it could be related to differences in Saturn's middle atmospheric thermal structure as compared to Jupiter, or to a more vigorous upper atmospheric dynamics driven perhaps by copious amounts of helium condensation in the interior of Saturn (Atreya, 1982).

Despite the tremendous breakthroughs by Voyager, ISO, and the HST, much about the nature of vertical mixing in the atmospheres of the giant planets remains mysterious. Some of that will surely change as Cassini instruments, particularly the ultraviolet, infrared, and the visible-infrared spectrometers (UVIS, CIRS and VIMS), carry out detailed global mapping and height distribution measurements of trace species in the atmosphere of Saturn. Only then would it be possible to know whether and how the vertical mixing varies from equator to the high latitudes including the auroral regions, from belts to the zones, and from troposphere to the middle and upper atmosphere of Saturn as it could indeed be far more complex than indicated by the abovementioned relationship. The Cassini orbiter measurements will greatly improve upon the data available from Voyager because of many factors, most notably, larger spectral range, inclusion of visible range, greater spectral resolution combined with higher sensitivity, significantly higher data rate for most of the relevant instruments, as well as the opportunity to observe possible temporal variations over Cassini's nominal four-year orbital tour of Saturn.

4. Clouds and condensible volatiles

Even on the Earth, clouds are a poorly understood component of the atmosphere. Attempts to fully characterize Jovian clouds using computational models are far beyond present capabilities, yet computational models still play an important part in the analysis of cloud systems on Jovian planets. Perhaps the most used such model is the equilibrium cloud condensation model (ECCM), first developed by Weidenschilling and Lewis (1973). We use an implementation that has undergone further development as described in Atreya and Romani (1985), and although we refer the reader to those works for full details of the ECCM, some very important points must be made here. The cloud densities calculated by an ECCM are much greater than any densities that would actually be expected in the Jovian atmosphere, since atmospheric dynamics would not normally support a continuous wet adiabatic ascent through the entire atmospheric column, and microphysical processes would lead to a reduction of the cloud density through precipitation. Nevertheless, the ECCM is accurate in predicting lifting condensation levels for the condensible volatiles, as is shown by the comparison between the observed NH_3 cloud base (750 mb (Banfield et al., 1998) see discussion of cloud observations) and the calculated cloud base (0.72 bar for solar N/H, and 0.75 bar for $1.2\times$ solar N/H). Although the lack of an accurate treatment of atmospheric dynamics and microphysical processes might seem to render the ECCM useless for comparison to the real Jovian atmosphere, these authors are unaware at present of any models that do feature a full treatment of both atmospheric dynamics and microphysics. Until such a comprehensive model is available, the ECCM can still be used as a description of the specific hypothetical case of a direct adiabatic ascent of Jovian air with condensation but no sedimentation of condensed cloud material.

Fig. 4 shows results of ECCM calculations for Jupiter, with $1\times$ solar and $3\times$ solar condensible volatile abundances in the left panel, and greatly depleted condensible volatiles on the right. In Fig. 5, Saturn's clouds are simulated assuming $1\times$ solar and $5\times$ solar condensible volatile abundances. The choice of 3 and 5 for the condensible volatile enrichment factors are for illustration purposes only. It follows, however, assumptions based on the icy planetesimal model of giant planet formation, discussed later in Section 5. Table 4 summarizes the cloud base pressure and temperature coordinates for the modeled solar and supersolar cases and also gives cloud condensate column densities for the model cases, as well as cloud locations and column densities for the nephelometer observations of the Galileo Probe site (Ragent et al. 1998).

Until the descent of the Galileo Probe, clouds on the giant planets were observed only by remote sensing. The probe was expected to greatly further our understanding of Jovian clouds by descending through all three predicted layers of clouds. Observations at visible wavelengths of Jupiter and Saturn confirm a cloud at pressure levels appropriate for a cloud of ammonia ice. Although, in principle, it is possible to look deeper into the atmosphere at visible wavelengths, the relatively large effects of scattering at these wavelengths generally tend to limit the usefulness of visible wavelengths for sensing very deep into the atmosphere. This is evident also from the recent Galileo orbiter imaging observations of Jupiter at visible and near infrared wavelengths (727, 756, 889 nm), which positively identify a nearly ubiquitous cloud with its base at 750 mb (presumably NH_3-ice), but see a deeper cloud at $p \geq 4$ bar (presumably H_2O-ice) only in one region northwest of the Great Red Spot (Banfield et al., 1998). The Galileo Probe's Nephelometer sensed

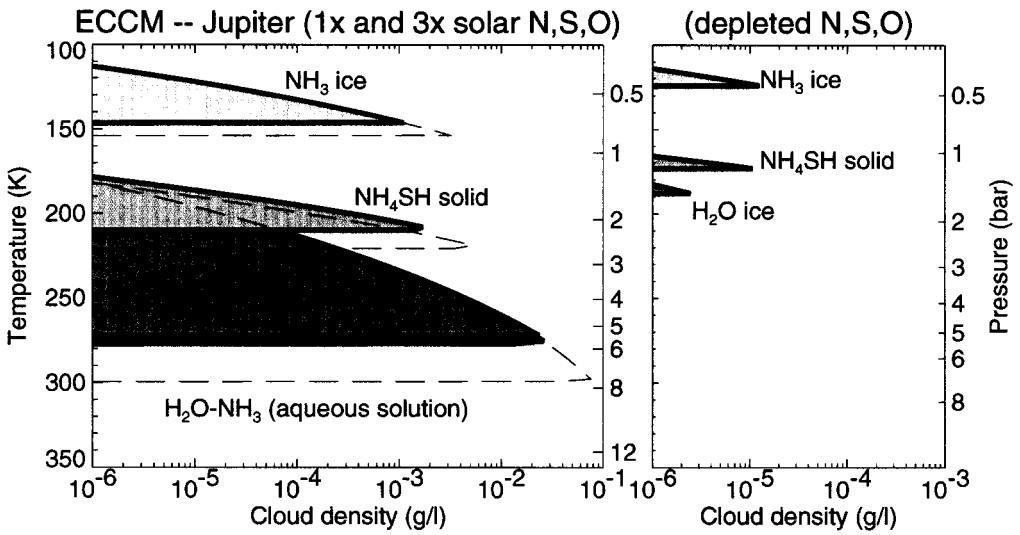

Fig. 4. (a, left) Jovian deep abundances of condensible volatiles were taken at 1 × solar (solid area) and 3 × solar (dashed lines) values (see Table 2), and used to calculate the equilibrium cloud densities. (b, right) As (a), but with the following depleted condensible volatile abundances relative to solar: H_2O: 0.01%; NH_3: 1%; H_2S: 0.5%.

only a tenuous cloud from 1.0 to 1.34 bar and possibly a thin layer at 1.6 bar (Ragent et al., 1998). Additional structures in the particle distribution were seen below this thin cloud, as well as in the 0.46–0.55 bar range. This latter structure could be the lower portion of an ammonia cloud, and is consistent with Net Flux Radiometer (NFR) measurements (Sromovsky et al., 1998), which also indicate the presence of a thin cloud at 0.5 bar. The most substantial structure, identified as a possible NH_4SH cloud, had an estimated particle mass loading of 7.6×10^{-4}–1.3×10^{-2} kg m^{-2}. Although this cloud may be speculated to be a possible NH_4SH cloud, it is important to note that the nephelometer could not measure the composition of cloud particles. Particles sensed by the nephelometer could be either the condensible volatiles discussed here or the poorly-understood chromophores, which might even be less volatile than the known condensible volatiles. The NH_4SH condensate column density predicted by the ECCM, for 2 × solar NH_3 and H_2S, is roughly 10 kg m^{-2}, but is expected to substantially overestimate actual particulate column densities, because it does not account for microphysical processes which eventually lead to loss of cloud particles through precipitation. Even so, it is clear that the clouds of the Galileo Probe region present an entirely different case than that described by the solar- or supersolar-abundance ECCM. Fig. 4b shows an ECCM calculation with

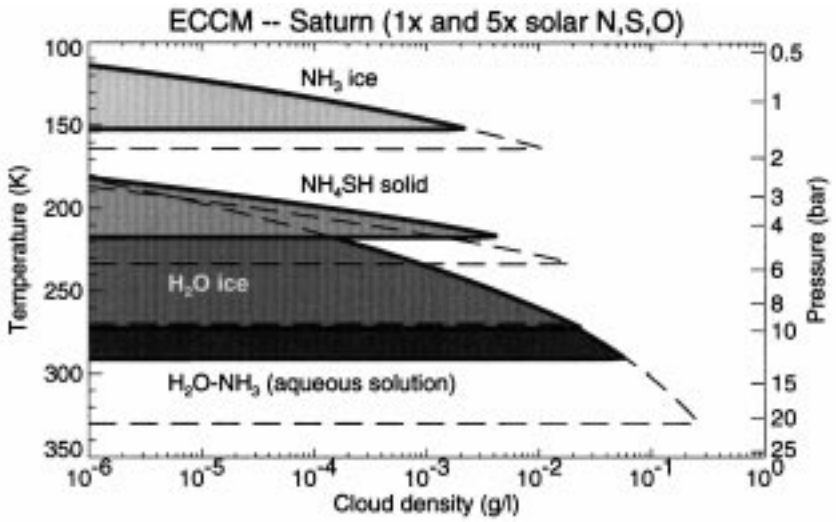

Fig. 5. Saturnian deep abundances of condensible volatiles were taken at 1 × solar (solid area) and 5 × solar (dashed lines) values (see Table 2), and used to calculate the equilibrium cloud densities.

Table 4
Modeled and observed cloud properties[a]

Case	Water cloud properties			NH_4SH cloud properties			Ammonia cloud properties		
	P (bar)	T (K)	ρ_c (kg m^{-2})	P (bar)	T (K)	ρ_c (kg m^{-2})	P (bar)	T (K)	ρ_c (kg m^{-2})
Saturn (solar CVs)	12.6	291	< 1600	4.56	217	< 38	1.47	152	< 20
Saturn (5 × solar CVs)	21.0	330	< 12000	5.72	233	< 206	1.81	164	< 117
Jupiter (observed in PES)[b]	2.45–3.58	247	$1.1–3.2 \times 10^{-4}$	1.0–1.34	176	7.6×10^{-4}– 1.3×10^{-2}	0.46–0.53	138	$0.3–5.7 \times 10^{-4}$
Jupiter (solar CVs)	5.69	277	< 251	2.21	210	< 6.6	0.72	146	< 3.6
Jupiter (3 × solar CVs)	7.22	299	< 958	2.61	221	< 22	0.84	154	< 12

[a] The modeled condensate column densities, ρ_c, should be regarded as upper limits since microphysical processes are expected to reduce them substantially (see text). Condensible volatiles are abbreviated as CVs. Pressure and temperature values are given at cloud base level. The mass loading, ρ_c, gives the condensate column density for the ECCM-calculated cloud or the observed cloud. In real atmospheric clouds, the cloud mass would be reduced substantially by microphysical processes leading to sedimentation.

[b] The observed cloud results are taken from the Galileo Nephelometer measurements of Ragent et al. (1998) for the Probe Entry Site (PES). Ranges in observed cloud pressure indicate extent of cloud; ranges in ρ_c indicate range in values consistent with the various data analysis procedures described in Ragent et al. (1998). The actual composition of the observed clouds is unknown, but the clouds are listed here under their assumed compositions. An additional thin cloud layer may be present at 1.6 bar level (Ragent et al., 1998), and it is consistent with the depleted abundance of water vapor at this level measured by GPMS (see Fig. 4b).

greatly depleted condensible volatile abundances relative to solar (H_2O: 0.01%; NH_3: 1%; H_2S: 0.5%, which are compatible with the probe measurements). The resulting clouds are in at least qualitative agreement with those measured by the nephelometer, and the particle mass loading of 1.8×10^{-2} kg m^{-2} of the main cloud (1.34 bar) in the model is in agreement with the upper range of the measured value for the cloud at this level. However, the comparison between these model results and the observed clouds should be taken with caution, since the sense of circulation for the two systems is probably quite different. The ECCM takes a parcel of air from the deep atmosphere and raises it up to the tropopause, whereas the probe site may be characterized by downward as well as horizontal motions (see discussion below). Although the ECCM is able to reproduce the observed cloud locations, and the required condensible volatile abundances are in agreement with those measured on the probe in the vicinity of the clouds, the model cannot reproduce the further increase of the condensible volatile mixing ratios at depths below the cloud bases.

The probe's descent, at 6.53° N planetocentric latitude and 0.94° W System III longitude (Young, 1998), was just within the location of an area of Jupiter known as a 5-μm hotspot. Orton et al. (1998b) estimate that the hotspot extended from about 11° W to 359° E and 5° to 8° N. The relative lack of clouds in 5-μm hotspots allows their emission to originate deeper in the Jovian atmosphere, thus making the hotspots appear much brighter than their surroundings, where the emission comes from a colder, higher altitude. These probe entry site conditions explain the peculiar discrepancy between the modeled and observed cloud structures.

Condensible volatile mixing ratios were also found to be markedly different from the ECCM scenario. The mixing ratio profiles of the three condensible volatiles (H_2O, H_2S, and NH_3) generally fit the same description: depleted values at the initial levels of the probe descent, followed by an increase with depth, culminating in a deep mixing ratio (for H_2S and NH_3) that was constant with depth (see Figs. 1 and 2). The recovery level, the pressure where the mixing ratio was seen to stop increasing with depth and remain constant, was different for the three condensible volatiles, and followed the sequence of the clouds predicted by the ECCM. The recovery levels of ammonia and hydrogen sulfide are 8 bars and 16 bars respectively (Table 1). The deepest measurement of water is 0.3 times solar with large uncertainties at 20.9 bar (see Table 1 and Niemann et al., 1998), but it seems likely that the probe did not reach the recovery level of water, so the abundance of water in Jupiter's well-mixed deep atmosphere is still unknown.

In order to simultaneously explain the difference between the modeled vs. the observed cloud and mixing ratio profiles, local meteorology in the form of a downdraft with entrainment has been invoked in numerous discussions (Atreya et al., 1996; 1997; Owen et al., 1996, 1997; Showman and Ingersoll, 1998). Downdraft systems had previously been considered to explain depleted water based on 5-μm remote sensing (see, for example, West et al., 1986). Column-stretching, as proposed in Showman and Ingersoll (1998), is a different mechanism that may explain the condensible volatile profiles without requiring horizontal mixing. The downdraft scenario, on the other hand, calls for a normal Jovian atmosphere as described by the ECCM, and downward flow of air in the probe region. The downdraft takes air from upper levels of the ambient atmosphere, which have been depleted of condensible volatiles through condensation and formation of the standard clouds, and forces this dry air downwards.

The downward movement of air, dried of its condensible volatiles through condensation, is a logical way to explain the depleted condensible volatile profiles of the probe region, since no tropospheric sources or sinks of these gases, other than cloud formation, have been established. But a useful model must also explain both the increase of the condensible volatiles with depth as well as their staggered recovery levels, which led many of the authors cited above to the straightforward conclusion that an additional process, such as horizontal mixing and entrainment, must operate in the hotspots.

One of the problems facing the downdraft scenario is the nature of the energy source needed to power it. Showman and Ingersoll (1998) examine a scenario where the entraining downdraft column is less dense than its surroundings, in order to explain the observed probe site condensible volatile mixing ratio profiles. They found that this scenario is thermally indirect, meaning that the downdraft circulation actually increases the potential energy of the atmosphere, or in other words, energy input is required to drive the downdraft. In addition, preliminary results of the downdraft with entrainment model of Wong et al. (1998) feature a downdraft whose thermally-direct phase ends no deeper than 2 bar. Both groups therefore must invoke external forcing in order to achieve a downdraft that extends as deep as the condensible volatile depletions observed by the Galileo Probe. Atreya et al. (1997) suggest a possibility that non-uniformities in the distribution of internal heat release might result in areas of reduced heat release, which would reduce the energy available to power convection and possibly facilitate a downdraft. Freidson et al. (1998) modeled a near-equatorial Rossby wave and found that under the right assumptions (such as the value of the Richardson number), phase differences between the wave vertical velocity and the total potential temperature gradient would produce localized conditions unstable to a downdraft, although more work must be done if this model is to accurately describe Jovian hot spots.

Although it seems clear that downdrafts, 5-μm hotspots, and the Galileo Probe descent path are related, several inconsistencies make the temporal and spatial structure of this relationship difficult to understand. Vertical motion of Jovian air is required to produce the depletions observed in the hotspots and the probe site, but sustained probe site vertical velocities are not supported by the Galileo Probe Atmospheric Structure Instrument: "Preliminary interpretation of the ASI data indicates alternating intervals of upwelling and downwelling of the vertical winds at the Galileo probe site" (Seiff et al., 1998). Galileo Orbiter Photopolarimeter/Radiometer measurements, sensitive at a resolution of 1600 km to the 300 mbar level (Orton et al., 1998a), did not show temperature contrasts in and out of hotspots. This result implies that any dynamic elements associated with 5-μm hotspots, such as downdrafts, cannot extend above the 300-mbar level. Wong et al. (1998) compared the probe site condensible volatile profiles to a downdraft model with parameterized entrainment, which extends the thunderstorm entraining downdraft model of Niewiadomski (1979) and includes condensation and evaporation of all three Jovian condensible volatiles. Preliminary results of the Wong et al. (1998) model are unable to simultaneously achieve modest downdraft velocities, condensible volatile profiles matching those of the probe site, and a depth of penetration of >5 bars. This growing body of contradictory observations, as well as contradictions between models and observations, seems to argue against an interpretation of 5-μm hotspots in terms of simplistic large-scale downdrafts. More successful interpretations may require smaller-scale dynamic elements such as interacting systems of small updrafts and downdrafts, and/or temporal variations such as brief rapid downdrafts followed by slower horizontal mixing, perhaps driven by near-equatorial Rossby waves (Friedson et al., 1998; Ortiz et al., 1998). Just such a short timescale (20 h), small spatial scale (15 km-wide downdraft plume), two-dimensional model with no condensible volatiles was presented by Baker and Schubert (1998). This 2D model features convective entrainment of a single discrete pocket of less-dense air, but substantial development will need to take place before it can be usefully compared to the widespread condensible volatile depletions found throughout the Galileo probe entry site and in Jovian 5-μm hotspots in general. Like the model of Wong et al. (1998), the Baker and Schubert (1998) model generates large downdraft velocities. In order to achieve much greater convective entrainment, as would be needed to explain large-scale condensible volatile depletions like those at the probe site, Baker and Schubert (1998) would need 'more vigorous convection', and therefore even more extreme vertical velocities. Nevertheless, this model may someday offer a clue to the solution of the mystery of Jovian hot spot dynamics.

Just as 5-μm hotspots yield the deepest glimpse of Jupiter's atmosphere, 5-μm bright regions of Saturn's atmosphere are our clearest window into that planet's deep atmosphere. Even though high contrast 5-μm hotspots are not observed on Saturn, Drossart (1998) reported a 1.5% saturated H_2O profile based on 5-μm ISO observations of Saturn (see Section 2 for additional explanation). Caution should be used with this result, since the H_2O saturated mixing ratio is only on the order of 150 parts per billion at the 3 bar level. Drossart's (1998) subsaturated profile for Saturn is similar to NIMS hot spot saturation profiles for Jupiter (Roos-Serote et al., 1998). Both ISO and the

Galileo Near Infrared Mapping Spectrometer (NIMS) observations disagree with the ECCM, which calls for condensible volatiles to follow their saturated profiles above the cloud bases (see Figs. 4 and 5). The implication is clear that similar processes may be depleting the condensible volatiles on both planets. Drossart's disk-averaged result is not necessarily an indication that water is everywhere depleted. Just as 5-μm spectra of Jupiter are strongly weighted toward hotspot emission, the ISO spectra may be weighted towards unknown regions of Saturn, which feature condensible volatile depletions produced by mechanisms similar to those operating on Jupiter.

5. Origin of the atmosphere

It is generally accepted that the cores of the giant planets, consisting of grains of rock (refractory material and metal) and ice formed first (Mizuno, 1980; Pollack and Bodenheimer, 1989). The circumplanetary solar nebula collapsed following the incorporation of the last of its gases, hydrogen, helium and neon, into the planetary envelope once the core mass became large enough for them to be gravitationally captured. It is believed that bombardment of icy planetesimals occurred throughout all phases of formation, and continued even after the planets had formed. Thus, the atmosphere we see today on the giant planets is believed to have resulted from outgassing from the core during accretionary heating, incoming planetesimals, and direct capture from the solar nebula. Therefore, this model implies an enhancement of the elemental abundances of those species that were trapped in the planetesimals and eventually released to the atmosphere.

The efficiency of trapping in ice depends upon the species and the temperature. The Interstellar Medium (ISM) can provide a clue to the primordial solar nebula. In the ISM, carbon is predominantly in the form of grains and refractory organics, not volatiles like CH_4 and CO. Similarly, grain reservoirs of many other heavy elements also far outweigh their volatile forms in the ISM. Such is not the case with nitrogen, however. Its main reservoir is in the volatile form, N_2, not in grains. Most of the comets in the Oort cloud are thought to have formed in the vicinity of Uranus and Neptune, i.e. at temperatures of 55 ± 15 K in the solar nebula. This is just above the lower limit of 30 ± 10 K on the molecule formation temperature in the pre-solar interstellar cloud, as determined from ion-molecule reactions that would reproduce observed values of D/H in H_2O and HCN in comet Hale-Bopp (Meier et al., 1998a; 1998b). However, a comet-formation temperature of 55 ± 15 K is consistent with temperatures derived from the relative abundances of CO/N_2, and C_2H_6/CH_4, as observed in comets (Owen and Bar-Nun, 1995; Notesco and Bar-Nun, 1996; Notesco et al., 1997). The difference between the temperatures derived from the isotopes and the trapped gases in comets may simply indicate that the icy grains falling into the solar nebula evaporated and recondensed at local temperatures, as modeled by Lunine et al. (1991). This process would not change the isotope ratios because there is not enough time (>4.5 Gyr required for equilibrium at these low temperatures). In other words the Oort cloud comets indicate two formation temperatures: one the formation of the molecules in the Interstellar Cloud from which the solar system formed, the other the temperature at which the icy grains recondensed in the solar nebula. Thus for grains that recondensed at larger solar distances than the Uranus–Neptune region, the solar nebula temperatures would have been lower, so that Kuiper Belt comets should consist of ice that reformed at the original interstellar cloud temperature of 30 ± 10 K.

Laboratory experiments have demonstrated that ice does not efficiently trap N_2, CO, and CH_4 near 55 K, but easily traps refractory organics and NH_3 as well as compounds of the other heavy elements (Bar-Nun et al., 1985; 1988). Thus we expect the Oort cloud comets that formed in the Uranus-Neptune region to be deficient in nitrogen, because they were unable to trap N_2, the major carrier of this element. This expected nitrogen deficiency has indeed been observed in comets (e.g., Wyckoff et al., 1991, Owen and Bar-Nun, 1995). Icy planetesimals that formed in the nebula at Jupiter's distance would have trapped even less N_2. Unless the temperature is below 25 K, ice does not trap Ne, and temperatures below 10 K are required to capture H_2 and He. These gases are not easily adsorbed in rocks either, so in Jupiter's atmosphere, we expect H, He and Ne to be contributed only by solar nebula gas and therefore to exhibit solar relative abundances. Contribution of nitrogen to the atmosphere by outgassing from the core or by infalling planetesimals should also be small. Thus, little enhancement in the nitrogen elemental ratio is expected. On the other hand, considerable enrichment in the abundances of carbon, sulfur and oxygen should occur. These conclusions rest on the assumption that most of the icy planetesimals contributing to Jupiter's growth and development formed at temperatures above 40 K. Obviously there will be some contribution from Kuiper Belt Objects (KBOs) that originated at lower temperatures. KBOs could carry more nitrogen and heavy noble gases than the planetesimals formed at higher temperatures and could thus produce some enrichment of even these species over their solar abundances.

The carbon and sulfur elemental abundances in Jupiter's atmosphere are, respectively, $2.9 \times$ solar and $2.5 \times$ solar (Table 2). The nearly equal enrichment of these elements is consistent with the predictions of a

model in which icy planetesimals make the major contribution of heavy elements (Owen and Bar-Nun, 1995; Owen et al., 1997; 1998). Even in the carbonaceous chondrites, the most carbon rich of the meteorites, C/S = 0.1 × solar. Unless there are 'rocky' bodies unsampled by our collection of meteorites that contain much more carbon, it appears, only icy planetesimals have the correct composition to enrich these elements almost equally (Owen et al., 1997; 1998). The icy planetesimal model also predicts that oxygen (as H_2O) should be similarly enhanced, perhaps even slightly more than carbon (Owen and Bar-Nun, 1995).

Unlike carbon and sulfur, enhancement of the nitrogen elemental ratio is not expected because of the difficulty of trapping nitrogen in ice unless the temperature is below 35 K (Owen and Bar-Nun, 1995). Therefore, there is an apparent contradiction between the predictions of the icy planetesimal model and the 3.6 × solar NH_3 mixing ratio derived by Folkner et al. (1998) for the deep atmosphere of Jupiter. If this measurement is correct, it would require that solid planetesimals bring in nitrogen, carbon and sulfur in nearly the same proportions we find in the sun, but we know of no planetesimals that have this composition, although Kuiper Belt comets may (Owen et al., 1998). The comets whose composition we have measured are deficient in nitrogen (Krankowsky, 1991; Wyckoff et al., 1991). Thus a value of N on Jupiter of 3.6 × solar would require building up the core and/or dominating the infalling ices with comets from the Kuiper Belt, or with solid material coming directly from the interstellar cloud that formed the solar system, without sublimation and recondensation as described by Lunine et al. (1991).

As we have seen, however, there is a fundamental contradiction between the Folkner et al. (1998) NH_3 mixing ratio and the radio spectrum of the planet (see Section 2). A possible solution might lie in the existence of an additional microwave absorber such as PH_3, as discussed earlier (Section 2). If this proves to be correct, then nitrogen could indeed be deficient, as the icy planetesimal model predicts.

Another constraint on this problem is provided by the abundances of the heavy noble gases. If N_2 was captured by the icy planetesimals that enriched the carbon and sulfur on Jupiter in sufficient amounts to provide a 3.6 × solar enrichment of N, the same enrichment should have occurred for argon, krypton and xenon. Otherwise, we expect these gases to be present in roughly solar proportions relative to hydrogen, enhanced somewhat by any planetesimals from the Kuiper Belt that might have struck the forming planet. This is exactly what the argon mixing ratio of $1.7 \pm 0.6 \times$ solar measured by the GPMS appears to demonstrate, but we should accept the caveat that some of the original argon may have joined the neon in those helium raindrops.

We must await the accurate determination of mixing ratios for both Kr and Xe to test this point further. However, at this stage we feel we can already rule out clathrate hydrate structures in the cometary ice as volatile carriers based on the predictions of Lunine and Stevenson (1985). Extrapolating from their published calculations for the enrichment of Xe and Kr as a function of the enrichment of carbon, we find for C/H = 3 × solar, Xe/Ar > 9 × solar for the least enhanced cases (Structure I clathrate, CH_4 dominant; Structure II clathrate, CO dominant). Instead, the present GPMS data on Xe and Ar give Xe/Ar ≤ 3 × solar in Jupiter's atmosphere (Table 2).

Finally, according to the icy planetesimal model, progressively greater enhancement of the elemental ratios of heavy elements is expected from Jupiter to Neptune. So far only the carbon elemental ratio has been measured in the atmospheres of all four giant planets. Despite the relatively large uncertainty in the determination of the methane mixing ratio at Saturn and beyond, there is no doubt about the trend — C/H increases from 2.9 × solar at Jupiter to roughly 6 × solar at Saturn (Tables 1 and 2), 25 × solar at Uranus and 35 × solar in Neptune's atmosphere (Baines et al., 1995). Cassini infrared instruments are expected to constrain the abundances of certain heavy element gases, such as CH_4, NH_3, and PH_3 quite well on Saturn. Elemental abundances of several other key elements, such as sulfur and oxygen, will continue to remain a mystery, however, even after Cassini.

6. Summary and conclusions

The ultimate ambitious goal of the exploration of the giant planets is to understand their formation and the origin and evolution of their atmospheres. This can be best accomplished by a comparative planetology approach. In this paper we have attempted to give the present status of certain key issues of the atmospheres of Jupiter and Saturn, including their comparative composition, vertical mixing, cloud structure, and origin. We have been guided in this pursuit by the wealth of observational results available from Voyager, Galileo, Infrared Space Observatory, Hubble Space Telescope and Earth-based telescopes. The strength of vertical mixing in Saturn's upper atmosphere is nearly a factor of 100 greater than on Jupiter, as evidenced by the eddy mixing coefficient at the homopause. The existing observations are mainly at low equatorial latitudes and correspond to a particular time during the Voyager epoch, however. In Saturn's atmosphere, observations from the Cassini–Huygens spacecraft are expected to result in a meaningful map

of the vertical mixing over this planet. The deep cloud structure of these planets will continue to be a mystery despite the exciting discoveries of Galileo and those expected from the Cassini–Huygens mission. This also implies that the abundance of water in the deep mixed atmosphere will not be determined beyond doubt, either. The elemental abundances of heavy elements, including oxygen (from water), are important to measure as they provide key constraints to the models of formation of the giant planets and their atmospheres. Carbon and sulfur elemental ratios have been determined accurately as a result of the Galileo probe measurements in the deep atmosphere of Jupiter, and they are both found to be supersolar. Although precise measurement of the methane mixing ratio on Saturn is expected from the Cassini orbiter infrared remote sensing observations, information on the hydrogen sulfide abundance will at best be model dependent. The elemental ratios of several other key elements will, however, be measured with varying degrees of accuracy; included in this list are N, P, Ge and As. The nitrogen elemental ratio in Jupiter's atmosphere is enigmatic, especially in view of the large discrepancy between the global ammonia abundance interpreted from the ground-based radio observations, which give essentially solar NH_3, and that inferred from the analysis of the Galileo probe-orbiter radio attenuation data, which yields nearly $4 \times$ solar NH_3 in the deep mixed atmosphere. This apparent discrepancy could conceivably result from an unknown microwave absorber, or some as yet mysterious effects in the modelling and interpretation of the microwave data. Eventually, should the nitrogen elemental abundance also turn out to be supersolar, it may warrant reexamination of certain aspects of the current hypothesis of the origin of Jupiter's atmosphere. The existing evidence, based on the supersolar elemental abundances of heavy elements, including C on all four giant planets and S on Jupiter, appears to favor the icy planetesimal model of the formation of the giant planets and the subsequent origin of their atmospheres. To understand this fundamentally important question beyond doubt will, however, require observations far beyond the capabilities of Galileo and Cassini–Huygens. Cleverly instrumented multiprobes into the atmospheres of Jupiter and Saturn could definitely revolutionize our thinking of how the giant planets and their atmospheres formed.

7. Note added in proof

Our improved analysis of the GPMS data now gives an argon elemental ratio of $2.1 \pm 0.4 \times$ solar in Jupiter's atmosphere. Moreover, further examination of ground-based microwave spectra, including the effects of synchrotron radiation and error analysis, has led us to conclude that these data are reliable down to approximately the 4-bar level, whereas the ammonia results from Galileo probe's radio attenuation experiment are good below this level. Hence, a supersolar value of N/H in the well-mixed part of Jupiter's atmosphere seems quite likely. These new developments, taken together with the supersolar C/H and S/H, point to the formation of Jupiter from very low temperature (≤ 30 K) icy planetesimals, as we discuss in a paper, "Low-temperature planetesimals are required to form Jupiter", by T.C. Owen, P.R. Mahaffy, H.B. Niemann, S.K. Atreya, A. Bar-Nun, T.M. Donahue, I. de Pater, *Nature*, 1999, in press.

Acknowledgements

We thank Robert A. West for his insightful comments on the manuscript. Discussions with Michael F. Flasar and Angioletta Coradini on the Cassini infrared and visible observation capabilities were helpful. This research was supported in part by grants from NASA's Planetary Atmospheres Program (SKA), Planetary Astronomy Program (I de P, TCO), and the Cassini–Huygens Project (SKA, HBN, TCO).

References

Anders, E., Grevesse, N., 1989. Abundances of the elements — meteoritic and solar. Geochim. Cosmochim. Acta 53, 197–214.

Atreya, S.K., 1982. Eddy diffusion coefficient on Saturn. Planet Space Sci. 30, 849–854.

Atreya, S.K., 1986. Atmospheres and Ionospheres of the Outer Planets and Their Satellites. Springer–Verlag, New York–Berlin, pp. 66–79 Chapter 4.

Atreya, S.K., Romani, P.N., 1985. Photochemistry and clouds of Jupiter, Saturn and Uranus. In: Hunt, G.E. (Ed.), Planetary Meteorology. Cambridge University Press, pp. 17–68.

Atreya, S.K., Donahue, T.M., Festou, M.C., 1981. Jupiter: structure and composition of the upper atmosphere. Astrophys. J. 247, L43–L47.

Atreya, S.K., Sandel, B.R., Romani, P.N., 1991. Photochemistry and vertical mixing. In: Bergstralh, J.T., Miner, E.D., Matthews, M.S. (Eds.), Uranus. University of Arizona Press, Tucson, AZ, pp. 110–146.

Atreya, S.K., Edgington, S.G., Encrenaz, Th, Feuchtgruber, H., 1999. ISO observations of C_2H_2 on Uranus and CH_3 on Saturn: implications for atmospheric vertical mixing in the Voyager and ISO epochs, and a call for relevant laboratory data. In: Cox, P., Kessler, M.F. (Eds.), Universe As Seen by Infrared Space Observatory, pp. 149–152 ESA SP-427.

Atreya, S.K., Owen, T.C., Wong, M.H., Niemann, H.B., Mahaffy, P.R., 1996. Condensible volatiles, clouds, and implications for meteorology in the Galileo probe entry region. Bull. Am. Astron. Soc 28, 1133.

Atreya, S.K., Wong, M.H., Owen, T.C., Niemann, H.B., Mahaffy, P.R., 1997. Chemistry and clouds of the atmosphere of Jupiter: a Galileo perspective. In: Barbieri, C., Rahe, J., Johnson, T., Sohus, A. (Eds.), Three Galileos: The Man, The Spacecraft, The

Telescope. Kluwer Academic Publishers, Dordrecht, The Netherlands, pp. 249–260.
Baines, K.H., Mickelson, M.E., Larson, L.E., Ferguson, D.W., 1995. The abundances of methane and ortho/para hydrogen on Uranus and Neptune: implications of new laboratory 4–0 quadrupole line parameters. Icarus 114, 328–340.
Baker, R.D., Schubert, G., 1998. Note: Deep convective entrainment by downdrafts in Jupiter's atmosphere. Icarus 136, 340–343.
Banfield, D., Gierasch, P.J., Bell, M., Ustinov, E., Ingersoll, A.P., Vasavada, A.R., West, R.A., Belton, M.J.S., 1998. Jupiter's cloud structure from Galileo imaging data. Icarus 135, 230–250.
Bar-Nun, A., Kleinfeld, I., Kochavi, E., 1988. Trapping of gas mixtures by amorphous water ice. Phys. Rev. B. 38, 7749–7754.
Bar-Nun, A., Herman, G., Laufer, D., Rappaport, M.L., 1985. Trapping and release of gases by water, ice and implications for icy bodies. Icarus 63, 317–332.
Baron, R., Joseph, R.D., Owen, T.C., Tennyson, J., Miller, S., Ballester, G.E., 1991. Imaging Jupiter's aurora from H_3^+ emissions in the 3–4 μm band. Nature 353, 539–542.
Bézard, B., 1998. Detection of new hydrocarbons on the giant planets. Bull. Am. Astron. Soc. 30, 1059.
Bézard, B., Feuchtgruber, H., Moses, J.I., Encrenaz, T., 1998. Detection of methyl radicals (CH_3) on Saturn. Astron. Astrophys. 334, L41–L44.
Bishop, J., Romani, P.N., Atreya, S.K., 1998. Voyager 2 ultraviolet spectrometer solar occultations at Neptune: photochemical modeling of the 125–165 nm lightcurves. Planet. Space Sci. 46, 1–20.
Bishop, J., Atreya, S.K., Herbert, F., Romani, P.N., 1990. Reanalysis of Voyager 2 UVS occultations at Uranus: hydrocarbon mixing ratios in the equatorial stratosphere. Icarus 88, 448–464.
Bjoraker, G.L., Larson, H.P., Kunde, V.G., 1986. The abundance and distribution of water vapor in Jupiter's atmosphere. Astrophysical Journal 311, 1058–1072.
Black, D.C., 1972. On the origins of trapped helium, neon, and argon isotopic variations in meteorites — I. Cosmochim. Acta 36, 347.
Broadfoot, A.L., Belton, M.J.S., Takacs, P.Z., Sandel, B.R., Shemansky, D.E., Holberg, J.B., Ajello, J.M., Atreya, S.K., Donahue, T.M., Moos, H.W., Bertaux, J.L., Blamont, J.E., Strobel, D.F., McConnell, J.C., Dalgarno, A., Goody, R., McElroy, M.B., 1979. Extreme ultraviolet observations from Voyager 1 encounter with Jupiter. Science 204, 979–982.
Caldwell, J.J., 1977. Ultraviolet observations of Mars and Saturn by the TD1A and OAO-2 satellites. Icarus 32, 190–209.
Carlson, B.E., Lacis, A.A., Rossow, W.B., 1993. Tropospheric gas composition and cloud structure of the Jovian North Equatorial Belt. J. Geophys. Res. 98, 5251–5290.
Combes, M., Maillard, J.P., de Bergh, C., 1977. Evidence for a telluric value of $^{12}C/^{13}C$ ratio in the atmospheres of Jupiter and Saturn. Astron. Astrophys. 61, 531–537.
Conrath, B.J., Gautier, D., Hanel, R.A., 1984. The helium abundance of Saturn from Voyager measurements. Astrophys. J. 282, 807–815.
Courtin, R., Gautier, D., Marten, A., Bézard, B., Hanel, R., 1984. The composition of Saturn's atmosphere at Northern temperate latitudes from Voyager IRIS spectra: NH_3, PH_3, C_2H_2, C_2H_6, CH_3D, CH_4, and the Saturnian D/H ratio. Astrophys. J. 287, 899–916.
de Boer, D.R., Steffes, P.G., 1994. Laboratory measurements of the microwave properties of H_2S under simulated Jovian conditions with an application to Neptune. Icarus 109, 352–366.
de Graauw, Th, Feuchtgruber, H., Bézard, B., Drossart, P., Encrenaz, Th, Beintema, D.A., Griffin, M., Heras, A., Kessler, M., Leech, K., Lellouch, E., Morris, P., Roelfsema, P.R., Roos-Serote, M., Salama, A., Vandenbussche, B., Valentijn, E.A., Davis, G.R., Naylor, D.A., 1997. First results of ISO SWS observations of Saturn: detection of CO_2, CH_3C_2H, C_4H_2 and tropospheric H_2O. Astron. Astrophys. 321, L13–L16.
de Pater, I., 1986. Jupiter's zone-belt structure at radio wavelengths. Icarus 68, 344–369.
de Pater, I., Massie, S.T., 1985. Models of the millimeter-centimeter spectra of the giant planets. Icarus 62, 143–171.
de Pater, I., Mitchell, D.L., 1993. Microwave observations of the planets: the importance of laboratory measurements. J. Geophys. Res. 98, 5471–5490.
de Pater, I., Romani, P.N., Atreya, S.K., 1989. Uranus' deep atmosphere revealed. Icarus 82, 288–313.
de Pater, I., Zahnle, K., Romani, P.N., 1999. Jupiter's deep atmosphere: a comparison of radio and Galileo probe data, J. Geophys. Res. (in preparation).
Drossart, P., 1998. Saturn tropospheric water measured with ISO/SWS. Bull. Am. Astron. Soc. 30, 1060.
Drossart, P., Encrenaz, Th, 1982. The abundance of water on Jupiter from the Voyager IRIS data at 5 micron. Icarus 52, 483–491.
Drossart, P., Fouchet, Th, Crovisier, J., Lellouch, E., Encrenaz, Th, Feuchtgruber, H., Champion, J-P., 1999. Fluorescence in the 3 micron bands of methane on Jupiter and Saturn from ISO/SWS observations. In: Cox, P., Kessler, M.F. (Eds.), Universe As Seen by Infrared Space Observatory, pp. 169–172 ESA SP-427.
Drossart, P., Maillard, J-P., Caldwell, J., Kim, S.J., Watson, J.K.G., Majewsky, W.A., Tennyson, J., Miller, S., Atreya, S.K., Clarke, J.T., Waite, J.H., Wagener, R., 1989. Detection of H_3^+ on Jupiter. Nature 340, 539–541.
Eberhardt, P., 1974. A neon-E-rich phase in the Orgueil carbonaceous chrondrite. Earth Planet. Sci. Lett. 24, 182.
Edgington, S.G., Atreya, S.K., Trafton, L.M., Caldwell, J.J., Beebe, R.F., Simon, A.A., West, R.A., 1999. Ammonia and eddy mixing variations in the upper troposphere of Jupiter from HST Faint Object Spectrograph observations. Submitted to Icarus.
Edgington, S.G., Atreya, S.K., Trafton, L.M., Caldwell, J.J., Beebe, R.F., Simon, A.A., West, R.A., Barnet, C., 1997. Phosphine mixing ratios and eddy diffusion coefficients in the troposphere of Saturn. Bull. Am. Astron. Soc. 29, 992.
Edgington, S.G., Atreya, S.K., Trafton, L.M., Caldwell, J.J., Beebe, R.F., Simon, A.A., West, R.A., Barnet, C., 1998. On the latitude variation of ammonia, acetylene, and phosphine altitude profiles on Jupiter from HST faint object spectrograph observations. Icarus 133, 192–209.
Encrenaz, Th, Combes, M., Zeau, Y., 1978. The spectrum of Jupiter between 10 and 13 microns: an estimate of the Jovian $^{14}N/^{15}N$ ratio. Astron. Astrophys. 70, 29.
Encrenaz, Th, Drossart, P., Feuchtgruber, H., Lellouch, E., Bézard, B., Fouchet, T., Atreya, S.K., 1999. The atmospheric composition and structure of Jupiter and Saturn from ISO observations: a preliminary review. Planet. Space Sci. 47, 1223–1240.
Encrenaz, Th, Feuchtgruber, H., Atreya, S.K., Bézard, B., Lellouch, E., Bishop, J., Edgington, S., de Graauw, Th, Griffin, M., Kessler, M.F., 1998. ISO observations of Uranus: the stratospheric distribution of C_2H_2 and the eddy diffusion coefficient. Astron. Astrophys. 333, L43–L46.
Festou, M.C., Atreya, S.K., Donahue, T.M., Sandel, B.R., Shemansky, D.E., Broadfoot, A.L., 1981. Composition and thermal profile of the Jovian atmosphere determined by the Voyager ultraviolet stellar occultation experiment. J. Geophys. Res. 86, 5715.
Feuchtgruber, H., Lellouch, E., de Graauw, Th, Bezard, B., Encrenaz, Th, Griffin, M., 1997. External source of oxygen in the atmospheres of the giant planets. Nature 389, 159–162.
Folkner, W.M., Woo, R., Nandi, S., 1998. Ammonia abundance in Jupiter's atmosphere derived from attenuation of the Galileo probe's radio signal. J. Geophys. Res. 103, 22,847–22,856.
Fouchet, Th, Lellouch, E., Encrenaz, Th, Drossart, P., Bezard, B.,

Feuchtgruber, H., de Graauw, Th, 1999. Observations of Jupiter with ISO/SWS: ammonia and hydrocarbons. In: Cox, P., Kessler, M.F. (Eds.), Universe As Seen by Infrared Space Observatory, pp. 177–180 ESA SP-427.

Freidson, A.J., Orton, G.S., Ortiz, J.L., 1998. Jovian 5-micron hot spots: downwelling induced by an equatorial Rossby wave. Bull. Am. Astron. Soc. 30, 1069.

Frommhold, L., Birnbaum, G., 1984. Hydrogen dimer structures in the F.I.R. spectra of Jupiter and Saturn. Astrophys. J. 283, L79–L82.

Gautier, D., Morel, P., 1997. A reestimate of the protosolar $(^2H/^1H)_p$ ratio from $(^1He/^4He)_{sw}$ solar wind measurements. Astron. Astrophys. 323, L9–L12.

Gautier, D., Owen, T., 1989. The composition of outer planet atmospheres. In: Atreya, S.K., Pollack, J.B., Matthews, M.S. (Eds.), Origin and Evolution of Planetary and Satellite Atmospheres. University of Arizona Press, Tucson AZ, pp. 487–512.

Gautier, D., Marten, A., Baluteau, J.P., Bachet, G., 1983. About unidentified features in the Voyager far infrared spectra of Jupiter and Saturn. Canad. J. Phys. 61, 1455–1461.

Geiss, J., 1993. Primordial abundance of hydrogen and helium isotopes. In: Prantzos, N., et al. (Eds.), Origin and Evolution of the Elements. Cambridge University Press, pp. 89–106.

Geiss, J., Reeves, H., 1972. Cosmic and solar system abundances of deuterium and helium-3. Astron. Astrophys. 18, 126.

Gillett, F.C., Low, F.J., Stein, W.A., 1969. The 2.8–14-micron spectrum of Jupiter. Astrophys. J. 157, 925–934.

Griffin, M.J., Naylor, D.A., Davis, G.R., Ade, P.A.R., Oldham, P.G., Swinyard, B.M., Gautier, D., Lellouch, E., Orton, G.S., Encrenaz, Th, de Graauw, Th, Furniss, H., Smith, I., Armand, C., Burgdorf, M., Di Giorgio, A., Ewart, D., Gry, C., King, K.J., Lim, T., Molinari, S., Price, M., Sidher, S., Smith, A., Texier, D., Trams, N., Unger, S.J., Salama, A., 1996. First detection of the 56-μm rotational line of HD in Saturn's atmosphere. Astron. Astrophys. 315, L389–L392.

Hanel, R., Conrath, B., Flasar, M., Kunde, V., Lowman, P., Maguire, W., Pearl, J., Perraglia, J., Samuelson, R., Gautier, D., Gierasch, P., Kumar, S., Ponnamperuma, C., 1979. Infrared observations of the Jovian system from Voyager 1. Science 204, 972.

Hoffman, J.P., Steffes, P.G., de Boer, D.R., 1999. Laboratory measurements of phosphine opacity: implications for planetary radio science. Icarus 140, 235–238.

Judge, D.L., Carlson, R.W., 1974. Pioneer 10 observations of the ultraviolet glow in the vicinity of Jupiter. Science 183, 317–318.

Kim, S.J., Caldwell, J., Rivolo, A.R., Wagener, R., Orton, G.S., 1985. Infrared polar brightness of Jupiter 3: spectrometry from the Voyager 1 IRIS experiment. Icarus 64, 233–248.

Kim, S.J., Drossart, P., Caldwell, J., Maillard, J-P., Herbst, T., Shure, M., 1991. Images of aurorae on Jupiter from H_3^+ emission at 4 μm. Nature 353, 536–539.

Kostiuk, T., Mumma, M.J., Espenak, F., Deming, D., Jennings, D.E., Maguire, E., Zipoy, D., 1983. Measurements of stratospheric ethane in the Jovian south polar region from infrared heterodyne spectroscopy of the ν_9 band near 12 μm. Astrophys. J. 265, 564–569.

Krankowsky, D., 1991. The composition of comets. In: Newburn Jr, R.L., Rahe, J., Neugebauer, M. (Eds.), Comets in the Post-Halley Era. Kluwer Academic Press, Norwell, Mass, pp. 855–877.

Kunde, V.G., Hanel, R.A., Maguire, W., Gautier, D., Baluteau, J.P., Maarten, A., Chedia, A., Husson, N., Scott, N., 1982. The tropospheric gas composition of Jupiter's north equatorial belt (NH_3, PH_3, CH_3D, GeH_4, H_2O) and the Jovian D/H isotopic ratio. Astrophys. J. 263, 443–467.

Larson, H.P., Davis, D.S., Hoffman, R., Bjoraker, G., 1984. The Jovian atmospheric window at 2.7 μm: a search for H_2S. Icarus 60, 621–639.

Lellouch, E., Drossart, P., Encrenaz, Th, 1989. A new analysis of the jovian 5-micron Voyager/IRIS spectra. Icarus 77, 457–465.

Lellouch, E., Feuchtgruber, H., de Graauw, Th, Encrenaz, Th, Bézard, B., Griffin, M., 1997. Deuterium and oxygen in the giant planets. In: Kessler, M. (Ed.), Proceedings of the First ISO Workshop on Analytical Spectroscopy, ESA-SP 419, Madrid, 6–8 October, pp. 131–135.

Lunine, J., Stevenson, D.J., 1985. Thermodynamics of clathrate hydrate at low and high pressures with application to the outer solar system. Astrophys. J. Suppl. 58, 493–531.

Lunine, J., Engel, S., Rizk, B., Horanyi, M., 1991. Sublimation and reformation of icy grains in the primitive solar nebula. Icarus 94, 333–344.

Mahaffy, P.R., Donahue, T.M., Atreya, S.K., Owen, T.C., Niemann, H.B., 1998a. Galileo probe measurements of D/H and $^3He/^4He$ in Jupiter's atmosphere. Space Science Rev. 84, 251–263.

Mahaffy, P.R., Niemann, H.B., Alpert, A., Atreya, S.K., Donahue, T.M., Owen, T.C., 1998b. Heavy noble gases in the atmosphere of Jupiter. Bull. Am. Astron. Soc. 30, 1066. Presented at the 30th DPS/AAS meeting, Madison, WI, October.

Meier, R., Owen, T.C., Jewitt, D.C., Matthews, H.E., Matthew, S., Biver, N., Bockelee-Morvan, D., Crovisier, J., Gautier, D., 1998a. A determination of the HDO/H_2O ratio in comet C/1995 01 (Hale-Bopp). Science 279, 842.

Meier, R., Owen, T.C., Jewitt, D.C., Matthews, H.E., Senay, M., Biver, N., Bockelee-Morvan, D., Crovisier, J., Gautier, D., 1998b. Deuterium in comet C/1995 O1 (Hale-Bopp): detection of DCN. Science 279, 1707.

Mizuno, H., 1980. Formation of the giant planets. Prog. Theor. Phys. 64, 544–557.

Niemann, H.B., Atreya, S.K., Carignan, G.R., Donahue, T.M., Haberman, J.A., Harpold, D.N., Hartle, R.E., Hunten, D.M., Kasprzak, W.T., Mahaffy, P.R., Owen, T.C., Way, S.H., 1998. The composition of the Jovian atmosphere as determined by the Galileo probe mass spectrometer. J. Geophys. Res. 103, 22,831–22,846.

Niemann, H.B., Atreya, S.K., Carignan, G.R., Donahue, T.M., Haberman, J.A., Harpold, D.N., Hartle, R.E., Hunten, D.M., Kasprzak, W.T., Mahaffy, P.R., Owen, T.C., Spencer, N.W., Way, S.H., 1996. The Galileo probe mass spectrometer: composition of Jupiter's atmosphere. Science 272, 846–849.

Niewiadomski, M., 1979. A numerical model of the updraft-downdraft interaction in Cb clouds. Acta Geophys. Polon. 27, 277–291.

Noll, K.S., Larson, H.P., 1990. The abundance of AsH_3 in Jupiter. Icarus 83, 494–499.

Noll, K.S., Larson, H.P., 1991. The spectrum of Saturn from 1990–2230 cm^{-1}: abundances of AsH_3, CH_3D, CO, GeH_4, and PH_3. Icarus 89, 168–189.

Noll, K.S., Knacke, R.F., Geballe, R.T., Tokunaga, A.T., 1988. The origin and vertical distribution of carbon monoxide on Jupiter. Astrophys. J. 324, 1210–1218.

Noll, K.S., Knacke, R.F., Tokunaga, A.T., Lacy, J.H., Beck, S., Serabyn, E., 1986. The abundances of ethane and acetylene in the atmospheres of Jupiter and Saturn. Icarus 65, 257.

Notesco, G., Bar-Nun, A., 1996. Enrichment of CO over N_2 by their trapping in amorphous ice and implications to comet P/Halley. Icarus 122, 118–121.

Notesco, G., Laufer, D., Bar-Nun, A., 1997. The source of the high C_2H_6/CH_4 ratio in comet Hyakutake. Icarus 125, 471–473.

Ollivier, J.L., Dobrijevic, M., Parisot, J.P., 1999. New photochemical model of Saturn's atmosphere. Planet. Space Sci., (submitted for publication).

Ortiz, J.L., Orton, G.S., Friedson, A.J., Stewart, S.T., Fisher, B.M., Spencer, J.R., 1998. Evolution and persistence of 5-μm hot spots at the Galileo probe entry latitude. J. Geophys. Res. 103, 23,051–23,069.

Orton, G.S., Tamppari, L.K., Fisher, B.M., Friedson, J., Martin, T., Travis, L.D., 1998a. High-resolution observations of Jupiter's 300-mbar temperature field by the PPR experiment from Galileo's Europa-16 orbit. Bull. Am. Astron. Soc. 30, 1074.

Orton, G.S., Fisher, B.M., Baines, K.H., Stewart, A.T., Friedson, A.J., Ortiz, J.L., Marinova, M., Ressler, M., Dayal, A., Hoffmann, W., Hora, J., Hinkley, S., Krishnan, V., Masanovic, M., Tesic, J., Tziolas, A., Parija, K.C., 1998b. Characteristics of the Galileo probe entry site from Earth-based remote sensing observations. J. Geophys. Res. 103, 22,791–22,814.

Orton, G., Ortiz, J.L., Baines, K., Bjoraker, G., Carsenty, U., Colas, F., Dayal, A., Deming, D., Drossart, P., Frappa, E., Friedson, J., Goguen, J., Golisch, W., Griep, D., Hernandez, C., Hoffmann, W., Jennings, D., Kaminski, C., Kuhn, J., Laques, P., Limaye, S., Lin, H., Lecacheux, J., Martin, T., Mccabe, G., Momary, T., Parker, D., Puetter, R., Ressler, M., Reyes, G., Sada, P., Spencer, J., Spitale, J., Stewart, S., Varsik, J., Warell, J., Wild, W., Yanamandra-Fisher, P., Fazio, G., Hora, J., Deutsch, L., 1996. Earth-based observations of the Galileo probe entry site. Science 272, 839–840.

Owen, T.C., Bar-Nun, A., 1995. Comets, impacts and atmospheres. Icarus 116, 215–226.

Owen, T.C., Westphal, J.A., 1972. The clouds of Jupiter: observational characteristics. Icarus 16, 392–396.

Owen, T.C., Meier, R., Bar-Nun, A., 1998. From the interstellar medium to planetary atmospheres via comets. In: Proceedings of a Faraday Discussion, No. 109, Faraday Society London, UK.

Owen, T.C., Atreya, S.K., Niemann, H.B., Mahaffy, P., 1996. The composition of Jupiter's atmosphere: implications for origin. EOS 77 (46), F438 Trans. Suppl.

Owen, T.C., Atreya, S.K., Mahaffy, P., Niemann, H.B., Wong, M.H., 1997. On the origin of Jupiter's atmosphere and the volatiles on the Medicean Stars. In: Barbieri, C., Rahe, J., Johnson, T., Sohus, A. (Eds.), Three Galileos: The Man, The Spacecraft, The Telescope. Kluwer Academic Publishers, Dordrecht, The Netherlands, pp. 289–297.

Owen, T.C., McKellar, A., Encrenaz, Th, Lecacheux, J., deBergh, C., Maillard, J., 1977. A study of the 1.56 micron NH_3 band on Jupiter and Saturn. Astron. Astrophys. 54, 291–295.

Parkinson, C.D., Griffoen, E., McConnell, J.C., Gladstone, G.R., Sandel, B.R., 1998. He 584 Å dayglow at Saturn: a reassessment. Icarus 133, 210–220.

Pollack, J.B., Bodenheimer, P., 1989. Theories of the origin and evolution of the giant planets. In: Atreya, S.K., et al. (Eds.), Origin and Evolution of Planetary and Satellite Atmospheres. University of Arizona Press, Tucson, AZ, pp. 564–604.

Ragent, B., Rages, K.A., Knight, T.C.D., Arvin, P., Orton, G.S., 1998. The clouds of Jupiter: results of the Galileo Jupiter mission probe nephelometer experiment. J. Geophys. Res. 103, 22,891–22,909.

Romani, P.N., de Pater, I., Zahnle, K., 1995. Galileo, SL9, and Jupiter's deep atmosphere. Bull. Am. Astron. Soc. 27, 81.

Roos-Serote, M., Drossart, P., Encrenaz, Th, Carlson, R.W., Leader, F., 1999. Constraints on the tropospheric cloud structure of Jupiter from spectroscopy in the 5-micron region: a comparison between Voyager/IRIS, Galileo/NIMS and ISO/SWS spectra. Icarus 137, 315–340.

Roos-Serote, M., Drossart, P., Encrenaz, Th, Lellouch, E., Carlson, R., Baines, K., Kamp, L., Orton, G., Muhlman, R., Calcutt, S., Irwin, P., Taylor, F., Weir, A., 1998. Analysis of Jupiter NEB hot spots in the 4–5 μm range from Galileo/NIMS observations: measurements of cloud opacity, water and ammonia. J. Geophys. Res. 103, 23,023–23,042.

Roulston, M.S., Stevenson, D.J., 1995. Prediction of neon depletion in Jupiter's atmosphere. EOS 76, F343 (abstract).

Sandel, B.R., McConnell, J.C., Strobel, D.F., 1982. Eddy diffusion at Saturn's homopause. Geophys. Res. Lett. 9, 1077–1080.

Seiff, A., Kirk, D.B., Knight, T.C.D., Young, R.E., Mihalov, J.D., Young, L.A., Milos, F.S., Schubert, G., Blanchard, R.C., Atkinson, D., 1998. Thermal structure of Jupiter's atmosphere near the edge of a 5-μm hot spot in the north equatorial belt. J. Geophys. Res. 103, 22,857–22,889.

Showman, A.P., Ingersoll, A.P., 1998. Interpretation of Galileo probe data and implications for Jupiter's dry downdrafts. Icarus 132, 205–220.

Smith, G.R., Shemansky, D.E., Holberg, J.B., Broadfoot, A.L., Sandel, B.R., 1983. Saturn's upper atmosphere from the Voyager 2 EUV solar and stellar occultations. J. Geophys. Res. 88, 8667–8678.

Spilker, T.R., 1990. Laboratory measurements of microwave absorptivity and refractivity spectra of gas mixtures applicable to giant planet atmospheres. PhD dissertation, Stanford University.

Spilker, T.R., 1993. New laboratory measurements on ammonia's inversion spectrum, with implications for planetary atmospheres. J. Geophys. Res. 98, 5539–5548.

Spilker, T.R., 1998. A general formalism for calculating radio opacity due to ammonia vapor in giant planet atmospheres. BAAS 30, 1067.

Sromovsky, L.A., Collard, A.D., Fry, P.M., 1998. Galileo probe measurements of thermal and solar radiation fluxes in the Jovian atmosphere. J. Geophys. Res. 103, 22,929–22,978.

von Zahn, U., Hunten, D.M., Lehmacher, G., 1998. Helium in Jupiter's atmosphere: results from the Galileo probe Helium Interferometer Experiment. J. Geophys. Res. 103, 22,815–22,829.

Weidenschilling, S.J., Lewis, J.S., 1973. Atmospheric and cloud structure of the Jovian planets. Icarus 20, 465–476.

Weisstein, E.W., Serabyn, E., 1996. Submillimeter line search in Jupiter and Saturn. Icarus 123, 23–36.

Weisstein, E.W., Serabyn, E., 1994. Detection of the 267 GHz $J = 1$–0 rotational transition of PH_3 in Saturn with a new Fourier transform spectrometer. Icarus 109, 367.

West, R.A., Strobel, D.F., Tomasko, M.G., 1986. Clouds, aerosols, and photochemistry in the Jovian atmosphere. Icarus 65, 161–217.

Wong, M.H., Atreya, S.K., Romani, P.N., 1998. Downdraft entrainment model. Bull. Am. Aston. Soc. 30, 1075. Presented at the 30th DPS/AAS meeting, Madison, WI, October.

Wyckoff, S., Tegler, S.C., Engel, L., 1991. Nitrogen abundance in comet Halley. Astrophys J. 367, 641–648.

Young, R.E., 1998. The Galileo probe mission to Jupiter: science overview. J. Geophys. Res. 103, 22,775–22,790.